NASA CONTRACTOR REPORT

NASA CR-1903

NASA CR-1903

ON CHEMICAL REACTIONS IN THE CHAR ZONE DURING ABLATION

by G. C. April, R. W. Pike, and E. G. del Valle

Prepared by
LOUISIANA STATE UNIVERSITY
Baton Rouge, La.
for Langley Research Center

NATIONAL AERONAUTICS AND SPACE ADMINISTRATION • WASHINGTON, D. C. • OCTOBER 1971

1. Report No.	2. Government Accession No.	3. Recipient's Catalog No.
NASA CR-1903		

4. Title and Subtitle	5. Report Date
ON CHEMICAL REACTIONS IN THE CHAR ZONE DURING ABLATION	October 1971
	6. Performing Organization Code

7. Author(s)	8. Performing Organization Report No.
G. C. April, R. W. Pike, and E. G. del Valle	
	10. Work Unit No.

9. Performing Organization Name and Address	11. Contract or Grant No.
Louisiana State University Baton Rouge, La.	NGR 19-001-016
	13. Type of Report and Period Covered
12. Sponsoring Agency Name and Address	Contractor Report
National Aeronautics and Space Administration Washington, D.C. 20546	14. Sponsoring Agency Code

15. Supplementary Notes

16. Abstract

The reacting flow of pyrolysis products through the char layer of low density, nylon phenolic resin, charring ablators and through porous graphite was studied experimentally and theoretically. It was found that a finite rate, reacting flow model is necessary to accurately describe the phenomena within char. The reaction kinetics for a temperature range of 500°F (533K) to 3000°F (1925K), with experimental simulation to 2300°F (1535K), were determined and incorporated into a mathematical model. This model, in conjunction with experimental results, was used to show the limitation of frozen and equilibrium flow in predicting the behavior within the char layer.

In addition, radioactive tracer studies using carbon-14 were conducted to determine carbon deposition and product distributions within the char. In general, deposition was greatest near the front surface where the temperature varied between 1800 - 2300°F (1252 - 1535K).

A bromine homogeneous gas phase catalyst was investigated as a means of increasing the energy absorption by chemical reactions. Excellent activity was observed. The temperature at which reactions started decreased from 1900°F (1312K) to 1500°F (1084K). This effect was measured by comparing the experimental exit gas compositions with compositions calculated by the non-equilibrium flow model using conventional kinetic data. Heterogeneous catalysts (molybdenum and tungsten) had essentially no effect on chemical reactions in the char.

17. Key Words (Suggested by Author(s))	18. Distribution Statement
Ablation Kinetics Catalysis in Ablation	Unclassified - Unlimited

19. Security Classif. (of this report)	20. Security Classif. (of this page)	21. No. of Pages	22. Price*
Unclassified	Unclassified	64	$3.00

*For sale by the National Technical Information Service, Springfield, Virginia 22151

NOMENCLATURE

English

A	Area
C_p	Heat capacity of a pure component at constant pressure
$\overline{C}_p$	Heat capacity of a mixture at constant pressure
c	Concentration of a component in the system
E	Energy of activation of a chemical reaction
H	Enthalpy of a component or mixture.
K	Total number of gas species in the system
k	Thermal conductivity of a pure component or reaction rate constant for a chemical reaction, see Table 1
k°	Frequency factor for a chemical reaction, see Table 1
L	Char Thickness
M_w	Molecular weight of a component in the system
m	Total number of chemical reactions in the system
n	Number of species in the system
P	Pressure
p	Stoichiometric coefficient of the products in a chemical reaction
p'	Power on the product concentration term for a chemical reaction
Q	Conductive, convective and radiative energy transfer rate
R	Ideal gas constant
$\overline{R}$	Effective chemical reaction rate for solid species
R_i	Chemical reaction rate of a species i
r'	Power on the reactant concentration term for a chemical reaction
s	Power on the temperature in the rate equation
T	Temperature
u	Velocity component in the x-coordinate direction
v	Velocity component in the y-coordinate direction

W Mass flux based on the superficial velocity

W_p Mass flux based on the velocity within the pore species

x Mass fraction

z Distance in the axial direction

Greek

β Inertial coefficient in the modified Darcy's equation

γ Permeability of a porous medium

Δ Forward difference operator

ϵ Porosity of a porous medium

$\bar{\epsilon}$ Emissivity of a porous medium

μ Viscosity of a pure component

ρ Density of a pure component

π Product operator

Subscripts

c Conductive or convective

cz Char zone

e Effective or overall value

f Fluid or gas phase

g Gas phase

L Front surface of the char

o Initial or inlet condition

P Pyrolysis or pores or pressure

r Radiation

rr Reradiation

T Temperature of total

z Distance from the back surface of the char

TABLE OF CONTENTS

SECTION I

INTRODUCTION

The charring ablator has proven to be one of the most successful thermal protection systems for reentry. These heat shields are a combination of plastics that decompose to a char or porous carbon and low molecular weight gases. Protection of the vehicle is achieved by conductive and convective heat transfer, plastic decomposition, transpiration, endothermic chemical reactions of the pyrolysis products, and reradiation from the char front surface. The charring ablator is conveniently divided into three separate zones which include the plastic decomposition layer, the char layer and the material-flow field interaction zone. Each of the above regions has been the subject of a sizeable research effort, and various types of mathematical models to describe the charring ablator have been developed (1,2,3).

In this research a better description of the phenomena taking place in the char zone is presented. An accurate description is needed of the energy transfer in the char and of the species compositions and fluxes entering the boundary layer. At present these are evaluated by considering the flow to be either frozen (no chemical reactions) or to be in chemical equilibrium.

For a more accurate description of the reacting flow in the char layer the kinetics of the chemical reactions must be included in solving the transport equations. The solution is more complex than the limiting cases because the species continuity equations must be solved also. Of all the possible reactions that could occur within the char over the temperature range encountered, those that actually occur must be selected and included in the analysis.

In addition, experiments must be conducted to assure that the theoretical model accurately predicts the energy transfer in the char layer. This can be achieved by flowing a mixture of compounds typical of the actual pyrolysis

gases through chars formed in arc-jet heaters. The chars can be radiantly heated to simulate the surface heating during reentry. Gases entering and leaving the char layer can be analysed to determine the extent of the reactions taking place. Thus the accuracy of the mathematical analysis can be assessed. Furthermore, the results of the analysis, referred to as the non-equilibrium model, can be compared with the limiting cases. In this way the approximations that result by assuming equilibrium or frozen flow are evaluated.

SECTION II

MATHEMATICAL MODEL

General Description

The momentum, energy and mass transfer associated with the flow of pyrolysis products through the char layer of a char-forming ablative plastic is considered. The pyrolysis products, formed by the thermal degradation of the plastic heat shield, enter the char zone at the decomposition temperature of the plastic. The products experience a temperature increase as they flow through the char and undergo thermal cracking to lower molecular weight species which react with each other and with the carbonaceous char layer. These predominantly endothermic reactions are important modes of energy absorption and must be included in any realistic analysis of the energy transfer in the char layer.

The mathematical model describing the transport phenomena taking place has the form of a one dimensional and steady flow. The pyrolysis gas products are considered to de ideal with physical and thermodynamic properties a function of temperature. Thermal equilibrium between the gases and the char is likewise assumed. Char porosity and permeability are considered constant, while the char thermal conductivity can vary with temperature. A schematic diagram indicating pyrolysis gas flow through a porous char zone is depicted in Fig. 1. As shown, the pyrolysis products enter the char at the decomposition temperature, T_o, and the exit at a higher front surface temperature, T_L. Changes in the mass flux of the various species within the char occur as a result of chemical reactions at finite reaction rates, R_i.

Because of the relatively high mass flux values experienced during reentry, a modified form of Darcy's equation including inertial contributions is used to calculated the pressure gradient ($P_o - P_L$) across the char. Energy

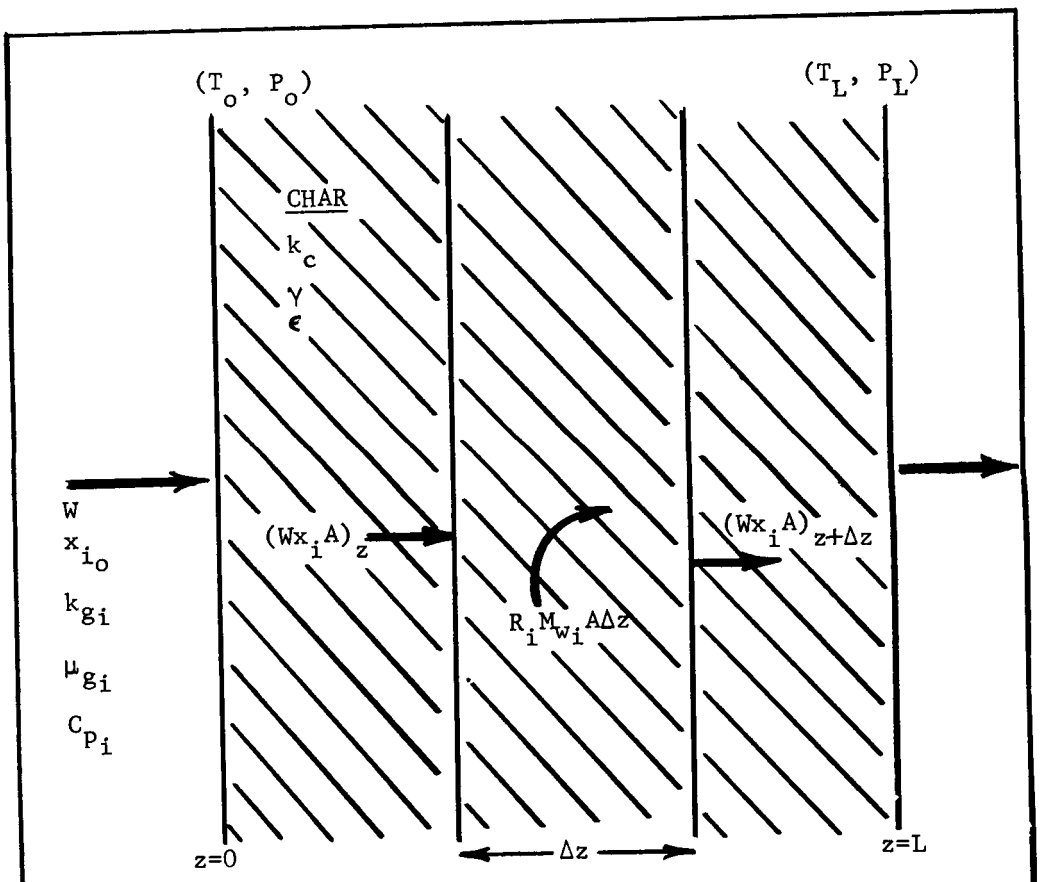

Figure 1. Schematic Diagram of the Char Zone.

transport by viscous dissipation, P-V work, diffusion and gravity are small and are not included in the model.

Equations of Change

To compute the energy transferred and the pressure distribution within a porous char, it is necessary to solve the energy and momentum equations with appropriate boundary conditions. For the restrictions stated above, the energy equation has the following form:

$$W_p \bar{C}_p \epsilon \frac{dT}{dz} = \frac{d}{dz}\left[k_e \frac{dT}{dz}\right] - \epsilon \sum_{i=1}^{K} H_i R_i - (1-\epsilon) H_c R_c \qquad (1)$$

To describe the pressure distribution, a modified form of Darcy's equation is used which accounts for inertial effects that are important due to relatively high mass fluxes of the degradation products. The following equation gives for the pressure at any point, z, within the char:

$$P = \left\{ P_L^2 + 2R \left[\int_z^L \left(\frac{\mu}{\gamma}\right)(W)\left(\frac{T}{M_w}\right) dz + \int_z^L \beta\left(\frac{T}{M_w}\right)(W)^2 dz \right] \right\}^{1/2} \qquad (2)$$

The energy absorbed in the char zone is equal to the difference between the heat flux at the high temperature surface and the heat flux at the back surface. Thus the net energy absorbed for nonequilibrium flow is calculated by the following heat flux equation:

$$Q_{cz} = (Q_L - Q_o) = \sum_{i=1}^{K} \int_{T_o}^{T_L} \epsilon W_p C_{Pi} x_i \, dT + \int_{T_o}^{T_L} (1-\epsilon)(H_c R_c)(dz/dT) \, dT \qquad (3)$$

A detailed derivation of the above equations is presented in Ref. 4.

Boundary Conditions

There are two sets of boundary conditions that are used to solve the

equations of change for flow of reacting gases within the char layer. The first set specifies the pressure and temperature at the front surface; and, the temperature and pyrolysis gas composition entering the back surface of the char.

$$T = T_L \ , \ P = P_L \text{ at } z = L \tag{4}$$

$$T = T_o \ , \ x_i = x_{io} \quad i = 1,2,\ldots,n \quad \text{at } z = 0 \tag{5}$$

These conditions for mass flux, W, as a parameter make the solution of the energy equation a two point boundary value problem. This requires an iterative solution. Because P-V work is negligible, the momentum equation is solved using an average pressure within the char. The heat flux at the char front surface is calculated using Eq. (3).

The second set of boundary conditions specified the temperature, initial pyrolysis gas composition and the sum of the heat of pyrolysis and the heat conducted in the virgin plastic (Q_p) at the back surface.

$$\begin{aligned} &T = T_o \\ &x_i = x_{io} \quad i = 1, z, \ldots n \quad \text{at } z = o \\ &Q_p = - k_e \, (dT/dz)_o \end{aligned} \tag{6}$$

For mass flux, W, and Q_p as parameters, the solution of the energy equation as an intial value problem is obtained for a specified char thickness. This does not require an iterative solution as did the first case. The heat flux at the surface is calculated using Eq. (3) as a function of the char thickness.

Application of the Equations to Nonequilibrium Flow

The application of the simplfied equations of change to nonequilibrium flow is different from the frozen and equilibrium flow models in the manner by which the term $H_i R_i$ is calculated in Eq. (1) and Eq. (3). For frozen

flow $H_i R_i$ is zero since there are no chemical reactions taking place. For flow in chemical equilibrium, the term $H_i R_i$ is not zero, and R_i, the reaction rate of species i, is calculated as a function of temperature and pressure by the method of free energy minimization (5). In the case of nonequilibrium flow of gases within the char, $H_i R_i$ term is again nonzero with R_i calculated from the species continuity equations.

For the jth chemical reaction, among species of chemical symbol A_i below

$$\sum_{i=1}^{n} r_{ij} A_i = \sum_{i=1}^{n} p_{ij} A_i \qquad j = 1,2,\ldots,m \tag{7}$$

the reaction rate, R_i, has the form of Eq. (8).

$$R_i = \sum_{j=1}^{m} (p_{ij} - r_{ij}) \left[k_{fj} \prod_{k=1}^{q} (c_k)^{p'_{kj}} - k_{rj} \prod_{k=1}^{q} (c_k)^{r'_{kj}} \right] \tag{8}$$

The ten chemical reactions which describe the reacting gas flow through the char between 500°F and 3000°F are listed in Table 1. A detailed discussion of the criteria used in arriving at these reactions is presented in Ref. 6.

In addition to the important chemical reactions, the initial pyrolysis gas composition must be specified as a boundary condition. The composition used in this research is based on the recent results reported by Sykes (7,8) and are shown in Table 2. These data represent the identification of approximately 90 percent of the total products released when a nylon-phenolic resin is thermally degraded. The simulated pyrolysis gas composition used in the experimental portion of this research is also listed in Table 2.

Physical and Thermodynamic Properties

In any problem where the temperature gradient varies over a wide range,

Table 1. Important Reactions and Associated Kinetic Data for the Pyrolysis Product Species in the Char Layer Between 500°f and 3000°F.

General Rate Constant Equation: $k = k^{\circ}T^{-s} \exp(-E/RT)$

No.	Reaction Formula	Rate Law	Activation Energy Kcal/gm-mole, E	Frequency Factor, k°	s
1.	$CH_4 \rightarrow 1/2\ H_2 + 1/2\ C_2H_6$	k_fA	95.0	7.6×10^{14} (a)	0
2.	$C_2H_6 \rightarrow C_2H_4 + H_2$	k_fA	70.0	3.1×10^{14} (a)	0
3.	$C_2H_4 \rightarrow C_2H_2 + H_2$	k_fA	40.0	2.6×10^{8} (a)	0
4.	$C_2H_2 \rightarrow 2\ C + H_2$	k_fA^2	10.0	2.1×10^{10} (b)	0
5.	$C + 2\ H_2 \rightarrow CH_4$	k_f	17.0	2.0×10^{9} (c)	0
6.	$C_6H_6O + H_2 \rightarrow H_2O + C_6H_6$	k_fA	45.0	2.0×10^{13} (a)	0
7.	$C_6H_6 \rightarrow 3\ C_2H_2$	k_fA	35.0	1.4×10^{9} (a)	0
8.	$C + H_2O \rightarrow CO + H_2$	k_fAB	82.0	1.2×10^{12} (b)	-1
9.	$CO + H_2O \rightarrow H_2 + CO_2$	k_fAB	30.0	1.0×10^{12} (b)	0
10.	$C + CO_2 \rightleftarrows 2\ CO$	$k_fA - k_rR^2$	50.0	1.0×10^{6} (a)	-1
			61.0	1.0×10^{-9} (b)	0

(a) First Order Reaction (sec^{-1})

(b) Second Order Reaction (cm^3/gm-mole-sec)

(c) Zeroth Order Reaction (gm-mole/cm^3-sec)

Table 2. Pyrolysis Products from the Thermal Decomposition of a Nylon-Phenolic Resin Composite Heat Shield

Component Identification	Composition, Mole Percent	
	Analysis of Sykes (7,8)	Simulated Pyrolysis Products
Dimethylphenol	1.2	0.0
Phenol	4.7	6.2
Benzene	0.1	0.0
Toluene	0.2	0.0
Water	48.9	48.9
Carbon Dioxide	1.1	1.1
Carbon Monoxide	3.7	3.7
Methane	6.7	6.7
Hydrogen	33.4	33.4
Total	100.0	100.0

changes in the physical and thermodynamic properties as a function of temperature occur. For the multicomponent flow of a reacting has within a porous char, composition change by chemical reactions is also important. The equations used in this investigation for calculating the variations in thermodynamic properties with temperature and composition are of the usual polynomial form found in the literature. Equations for the viscosity and thermal conductivity of gases are of the form presented by the Chapman-Enskog and Chapman-Cowling treatments, respectively. Details are presented in Ref. 4.

The Numerical Solution of the Equations of Change

The solution of the equations applied to the nonequilibrium flow of pyrolysis products within a porous char was obtained by numerical techniques on an IBM 360/65 computer. The specific techniques used were a fourth order Runge-Kutta formula for the solution of the differential energy and species continuity equations, and Simpson's Rule for the solution of the differential momentum and heat flux equations. In the case of nonequilibrium flow, the energy and species continuity equations were solved simultaneously because of the interdependence of the temperature and species concentrations.

SECTION III

CHAR ZONE THERMAL ENVIRONMENT SIMULATOR

The experimental data presented in this study were obtained using an apparatus that simulated the flow of pyrolysis gases through the char layer. Low density, nylon-phenolic resin chars were obtained from the National Aeronautics and Space Administration's Entry Structures Branch at the Langley Research Center. These specimens were placed in a metal holder with the front surface exposed to a bank of infrared quartz lamps used to simulate the high temperatures experienced by a reentering vehicle. Simulated pyrolysis gases were passed through the char from the rear surface to the heated front surface. The exit gases were sampled and analysed for comparison with the inlet gas composition to determine the extent of chemical reaction within the char. These results were also compared with the calculated exit gas compositions for frozen, equilibrium and non-equilibrium flow conditions. Thus this method determined the accuracy of the nonequilibrium model for predicting the flow of reacting pyrolysis gases in the char layer. A schematic diagram of the Char Zone Thermal Environment Simulator is shown in Fig. 2. A detailed description of the equipment, including dimensions, materials of construction and assembly diagrams are given in Ref. 4.

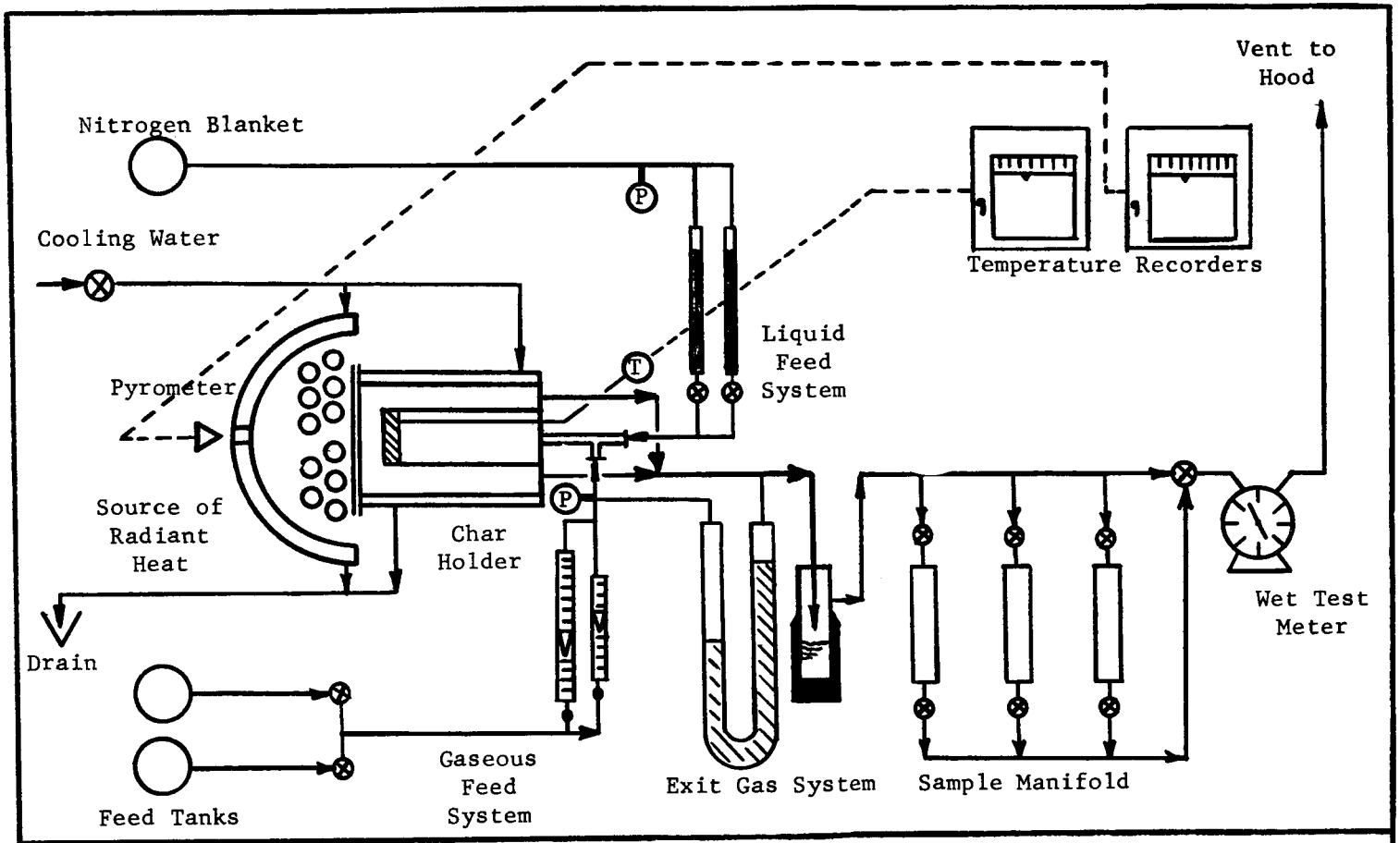

Figure 2. Schematic Diagram of the Char Zone Thermal Environment Simulator

SECTION IV

RESULTS OF THE NONEQUILIBRIUM ANALYSIS

Comparison of the Nonequilibrium Analysis with Experimental Data

The basis for evaluating the nonequilibrium flow model as an accurate and realistic analysis of energy transfer in the char layer is the comparison of the experimentally determined exit product compositions from the Char Zone Thermal Environment Simulator with the calculated compositions in the nonequilibrium flow model. This was done for seventeen experiments using low density, nylon-phenolic resin chars in which front surface temperatures of 1550°F to 2300°F (1090-1535°K) and pyrolysis gas mass flux values of 0.00003-0.108 lb/ft^2-sec (0.00015-0.540 kg/m^2-sec) were investigated.

In order to obtain significant conversion of the pyrolysis gases over the temperature range studied, the residence time within the porous char was increased by decreasing the mass flux. Thus the combination of the highest temperature and lowest mass flux produced the largest conversion resulting from chemical reactions.

Typical experimental results for the entire range of parameters studied are presented in Table 3. Also listed are the exit gas compositions resulting from the frozen (or initial composition), equilibrium and nonequilibrium flow analyses. The excellent agreement of the calculated nonequilibrium compositions with the experimentally determined exit gas composition obtained in the Char Zone Thermal Environment Simulator prove the analysis to be realistic and accurate over the range of temperature and mass flux values investigated. In addition, a definite transition from the frozen condition, corresponding to relatively low temperatures and high mass fluxes, to a nonequilibrium condition, corresponding to higher temperatures and lower mass fluxes, is noted. Also, in all cases except those in which the mass flux values were extremely

Table 3. Comparison of Calculated and Experimental Exit Gas Compositions for Pyrolysis Gas Flow Through a One-quarter Inch, Low Density, Nylon-Phenolic Resin Char at Mass Fluxes Between 0.00003 (0.00015) - 0.108 lb/ft^2-sec (0.540 Kg/m^{2}sec) and Front Surface Temperatures Between 1550°F (1170°K) and 2300°F (1533°K).

Run Number:	V-11				XVIII-58				XIX-60				XX-64				XVI-48			
Mass Flux: lb/ft^{2}sec (Kg/m^{2}sec)	0.0014 (0.0070)				0.1080 (0.540)				0.00248 (0.0125)				0.00103 (0.00515)				0.00003 (0.00015)			
Front Surface Temperature: °F (°K)	1550 (1117)				1680 (1190)				2030 (1383)				2300 (1533)				2055 (1397)			
Back Surface Temperature: °F (°K)	730 (661)				690 (639)				1375 (1019)				1190 (917)				1260 (956)			
Flow Model:	(a)	(b)	(c)	(d)	(a)	(b)	(c)	(d)	(a)	(b)	(c)	(d)	(a)	(b)	(c)	(d)	(a)	(b)	(c)	(d)
Exit Gas Composition (Mole %):																				
Hydrogen	37.2	71.6	37.2	37.0	30.6	59.5	30.6	30.8	29.3	62.7	38.2	41.3	28.4	65.9	25.2	26.7	31.7	83.1	84.7	84.5
Methane	32.5	1.4	32.5	32.0	6.2	3.5	6.2	6.1	6.0	0.8	17.2	18.2	5.4	0.3	25.6	26.4	46.3	0.4	8.2	7.7
Carbon Monoxide	8.2	14.9	8.2	8.5	3.5	26.0	3.5	3.4	3.3	35.2	25.2	23.4	3.4	33.6	38.5	40.3	5.5	7.0	2.9	3.0
Carbon Dioxide	6.6	0.1	6.6	6.4	1.0	4.4	1.0	1.1	0.9	1.5	8.8	7.6	1.0	0.0	0.9	0.6	2.5	0.0	0.0	0.6
Nitrogen	15.5	11.4	15.5	15.5	0.0	0.0	0.0	0.0	0.0	0.0	0.0	0.0	0.0	0.0	0.0	0.0	14.0	9.4	3.8	4.2
Water	0.0	0.6	0.0	0.0	51.9	6.5	51.9	50.8	53.7	0.9	4.9	5.0	46.0	0.2	0.0	0.0	0.0	0.1	0.0	0.0
Phenol	0.0	0.0	0.0	0.0	6.8	0.0	6.8	5.8	6.8	0.0	5.1	4.6	15.8	0.0	7.9	7.1	0.0	0.0	0.0	0.0
Ethylene	0.0	0.0	0.0	0.1	0.0	0.0	0.0	0.0	0.0	0.0	0.0	0.0	0.0	0.0	0.5	0.4	0.0	0.0	0.1	0.0
Acetylene	0.0	0.0	0.0	0.5	0.0	0.0	0.0	0.0	0.0	0.0	0.5	0.0	0.0	0.0	1.3	1.0	0.0	0.0	0.3	0.4
Pressure Drop Across Char (lb/ft^2):	0.5	0.5	0.5	0.7	22.0	18.8	22.0	17.5	0.7	0.6	0.6	0.7	0.2	0.3	0.2	0.2	0.0	0.0	0.1	0.1
Calculated Heat Flux (BTU/ft^2-sec):	0.9	13.1	0.9	-	69.8	735.2	69.8	-	1.2	13.0	2.4	-	1.1	32.5	1.2	-	0.01	0.3	0.03	-

(a) Frozen Flow Model (b) Equilibrium Flow Model (c) Nonequilibrium Flow Model (d) Experimental Data - Char Zone Thermal Environment Simulator

small (less than 0.0015 kg/m^2-sec), the compositions predicted by the equilibrium flow model were inaccurate and unrealistic. A more direct comparison of the three models will be discussed in the following section with emphasis on the shortcomings of the two ideal flow cases (frozen and equilibrium analyses).

Comparison of the Nonequilibrium Analysis with the Ideal Models

The frozen and equilibrium flow models bracket the nonequilibrium case. Frozen flow corresponds to a system in which no chemical reactions occur, while equilibrium flow refers to a system of species undergoing chemical reactions which are at equilibrium. Since the nonequilibrium flow model more accurately predicts the behavior, comparison of the exit gas compositions, temperature and pressure distribution, and surface heat flux for each model will determine the accuracy of the two limited flow analyses in predicting the energy transfer within the char layer.

These results are presented in Fig. 3 and Table 4 for a mass flux of 0.05 lb/ft^2-sec (0.25 kg/m^2-sec), a front surface temperature of 1500°F (1090°K) and a back surface temperature of 500°F (533°K). The char porosity is 0.8 and the char thickness is 0.25 inches (0.0064m). As seen the temperature profile of the nonequilibrium flow analysis is identical to the frozen flow temperature profile. The relative closeness of these two models at these conditions is likewise seen by comparing the exit gas compositions, pressure drop across the char and surface heat flux in Table 4. There is little evidence of chemical reactions in the char and the energy transfer is closely predicted by the frozen flow model.

In Fig. 4 and Table 5, the same results are presented for a front surface temperature of 2000°F (1368°K). Although the reported nonequilibrium values are again nearly equal to the frozen flow results, a noticeable change, especially in the concentration profiles and surface heat flux, is observed.

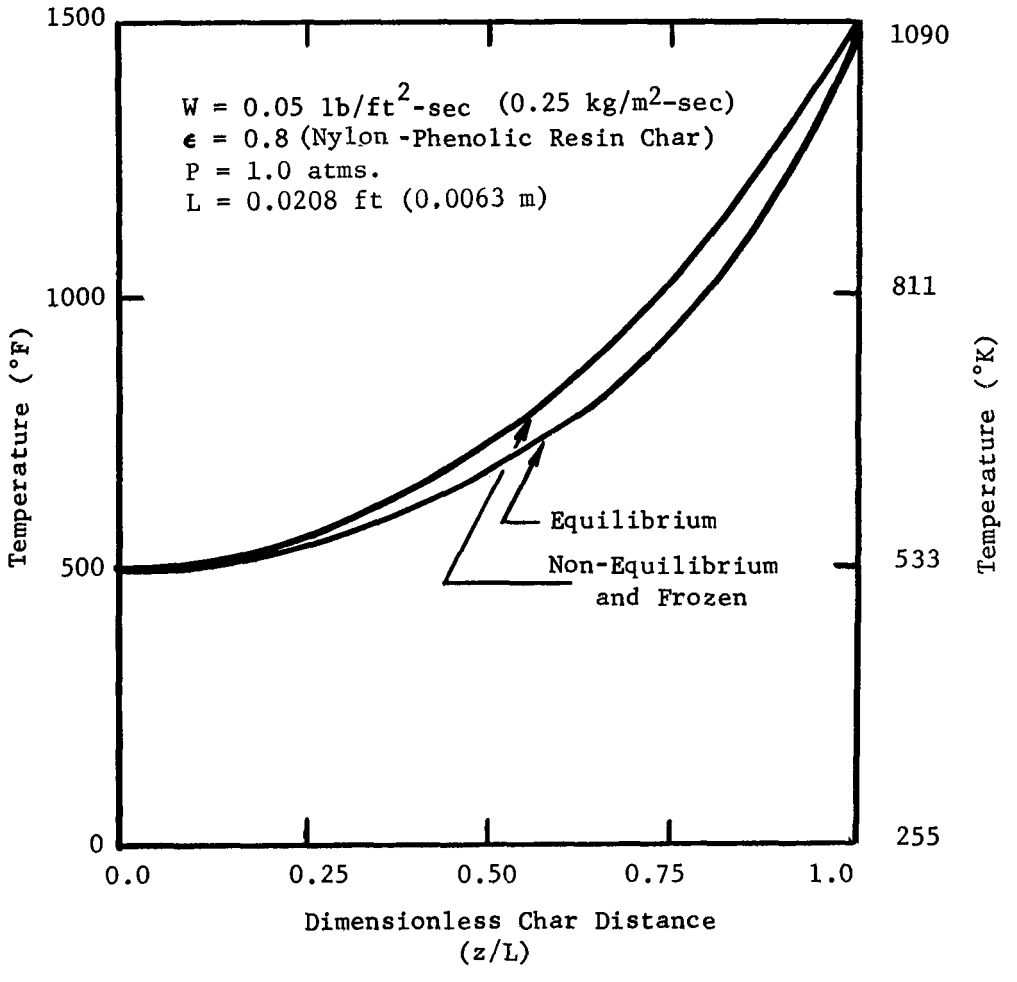

Figure 3. Temperature Profile for the Frozen, Equilibrium, and Non-Equilibrium Flow of Pyrolysis Gases Through the Char Zone of a Nylon-Phenolic Resin Ablator.

Table 4. Results of the Frozen, Equilibrium and Nonequilibrium Flow Analyses for Pyrolysis Gas Flow Through a One-Quarter Inch Low Density Nylon-Phenolic Resin Char at 1500°F (1090K), T_L.

Conditions: $W = 0.05$ lb/ft^{2}sec (0.25 kg/m^{2}sec), $\epsilon = 0.8$, $L = 0.0208$ ft (0.0063 m), $T_o = 500°F$ (533°K), $T_L = 1500°F$ (1090°K)

Char Position:	Inlet	Exit (z/L) = 1		
Flow Model:	All	Frozen	Equilibrium	Nonequilibrium
Composition (Mole%):	33.4	33.4	12.6	33.4
Hydrogen	6.7	6.7	31.8	6.7
Phenol	6.2	6.2	0.0	6.2
Water	48.9	48.9	45.8	48.9
Carbon Monoxide	3.7	3.7	0.2	3.7
Pressure Drop (lb/ft^2):	-	5.8	5.3	5.9
(kg/m^2)	-	29.0	26.5	29.5
Heat Flux (BTU/ft^2-sec):	-	31.8	46.3	31.9
(KJ/m^2-sec)	-	340.0	509.7	350.4

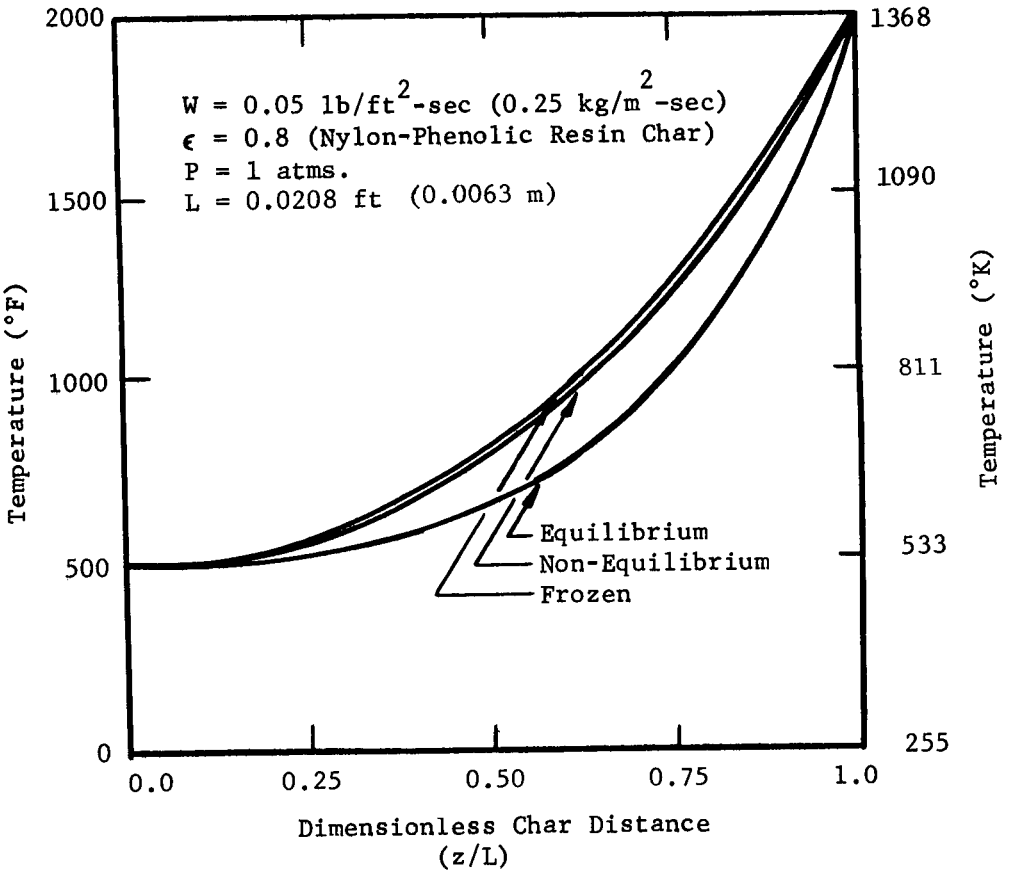

Figure 4. Temperature Profile for the Frozen, Equilibrium, and Non-Equilibrium Flow of Pyrolysis Gases Through the Char Zone of a Nylon-Phenolic Resin Ablator.

Table 5. Results of the Frozen, Equilibrium and Nonequilibrium Flow Analyses for Pyrolysis Gas Flow Through a One-Quarter Inch Low Density Nylon-Phenolic Resin Char at 2000°F (1368°K), T_L.

Conditions: $W = 0.05$ lb/ft^{2}sec, (0.25 kg/m^{2}sec); $\epsilon = 0.8$; $L = 0.0208$ ft, (0.0063m); $T_o = 500°F$ (533°K); $T_L = 2000°F$ (1368°K)

Char Position:	Inlet	Exit (z/L) = 1		
Flow Model:	(All)	Frozen	Equilibrium	Nonequilibrium
Composition (Mole %):				
Hydrogen	33.4	33.4	28.3	34.7
Methane	6.7	6.7	23.4	6.7
Phenol	6.2	6.2	0.0	6.2
Water	48.9	48.9	36.2	47.4
Carbon Monoxide	3.7	3.7	1.0	3.2
Carbon Dioxide	1.1	1.1	11.1	2.0
Pressure Drop (lb/ft^2):	-	7.2	6.0	7.2
(kg/m^2):	-	36.0	30.0	36.0
Heat Flux (BTU/ft^{2}sec):	-	50.1	98.3	50.5
(KJ/m^2-sec):	-	550.8	1081.5	555.7

This indicates chemical reactions among species within the char layer.

A continuation of the analysis to front surface temperatures of 2500°F (1645°K) (Fig. 5 and Table 6) and 3000°F (1925°K) (Fig. 6 and Table 7) shows a more dramatic change which is reflected by a downward shift of the non-equilibrium temperature profile toward the equilibrium curve and corresponding rapid changes in the concentration profiles and heat fluxes. Chemical reactions are obviously a very important mode of energy absorption under these last two sets of conditions.

It is not possible to extend the nonequilibrium analysis to temperatures above 3000°F (1925°K) since the chemical behavior within the char will not be predicted by the chemical reactions in Table 1. In this event additional reactions must be included to accurately describe the energy transfer within the char layer.

Parametric Study of Reacting Gas Flow in the Char Layer

A comparison of the nonequilibrium flow results with the experimental data was important in determining the accuracy of the flow model. However, very little quantitative information, beyond the discrete sets of data for each experiment, was assembled regarding the effect of changing mass flux and/or temperature. As a result, a parametric study was undertaken to accurately relate the changes in these variables with variations in energy absorption within the char. To do this the intial value problem was solved in which the back surface temperature and temperature gradient were specified as boundary conditions for various values of the mass flux. The results of the calculations were in the form of the net heat transfer at the surface, called the approximate aerodynamic heating, which was the sum of the surface heat flux and radiant heat flux resulting from the calculated front surface temperature:

$$Q_a = -k_e \left.\frac{dT}{dz}\right|_{z=L} + \bar{\epsilon}\sigma T_L^4 \qquad (9)$$

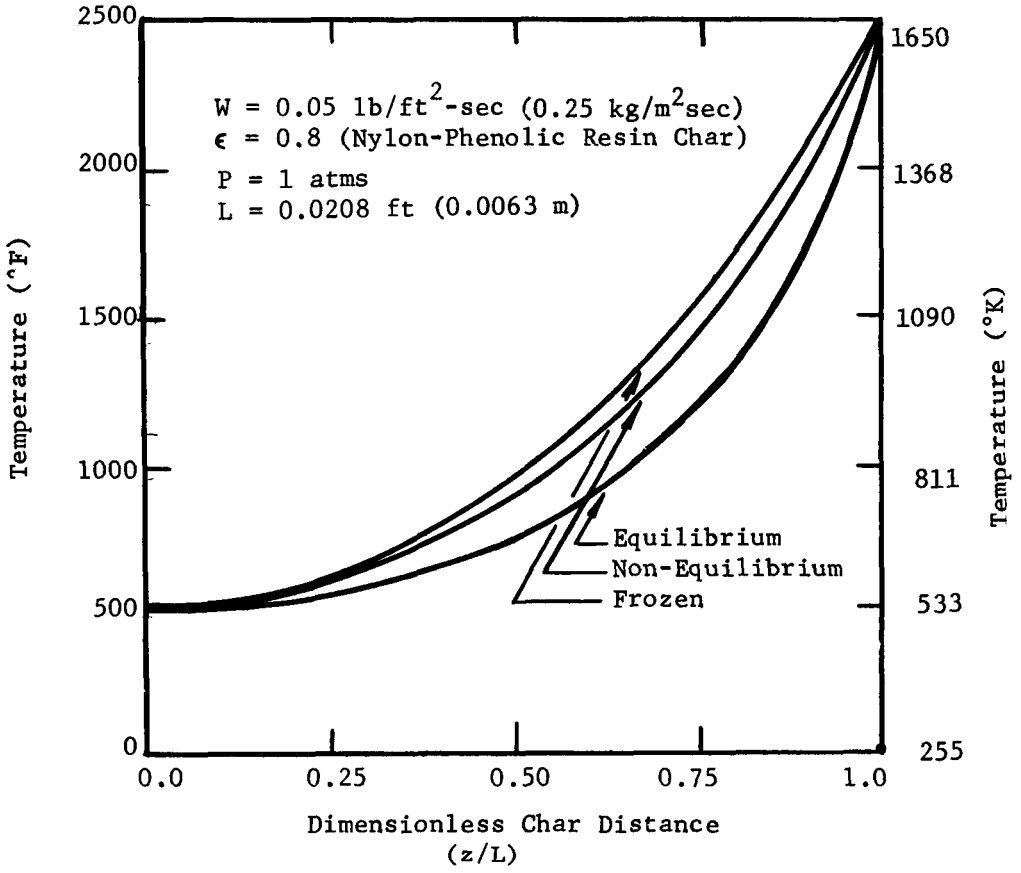

Figure 5. Temperature Profile for the Frozen, Equilibrium, and Non-Equilibrium Flow of Pyrolysis Gases Through the Char Zone of a Nylon-Phenolic Resin Ablator.

Table 6. Results of the Frozen, Equilibrium and Nonequilibrium Flow Analyses for Pyrolysis Gas Flow Through a One-Quarter Inch Low Density Nylon-Phenolic Resin Char at (1650°K).

Conditions: $W = 0.05$ lb/ft^{2}sec (0.25 kg/m^2-sec) $\epsilon = 0.8$, $L = 0.0208$ft (0.0063m) $T_o = 500°F$ ($533°K$) $T_L = 2500°F$ ($1650°K$)

Char Position:	Inlet	Exit (z/L) = 1		
Flow Model:	(All)	Frozen	Equilibrium	Nonequilibrium
Composition (Mole %):				
Hydrogen	33.4	33.4	55.7	53.8
Methane	6.7	6.7	7.8	5.1
Phenol	6.2	6.2	0.0	4.7
Water	48.9	48.9	19.2	9.0
Carbon Monoxide	3.7	3.7	5.5	21.7
Carbon Dioxide	1.1	1.1	11.8	5.6
Pressure Drop (lb/ft^{2}sec)	-	9.1	6.7	9.0
(kg/m^2):	-	45.5	33.5	45.0
Heat Flux (BTU/ft^{2}sec)	-	70.2	192.6	110.7
(KJ/m^2-sec):	-	2771.7	2118.7	1217.5

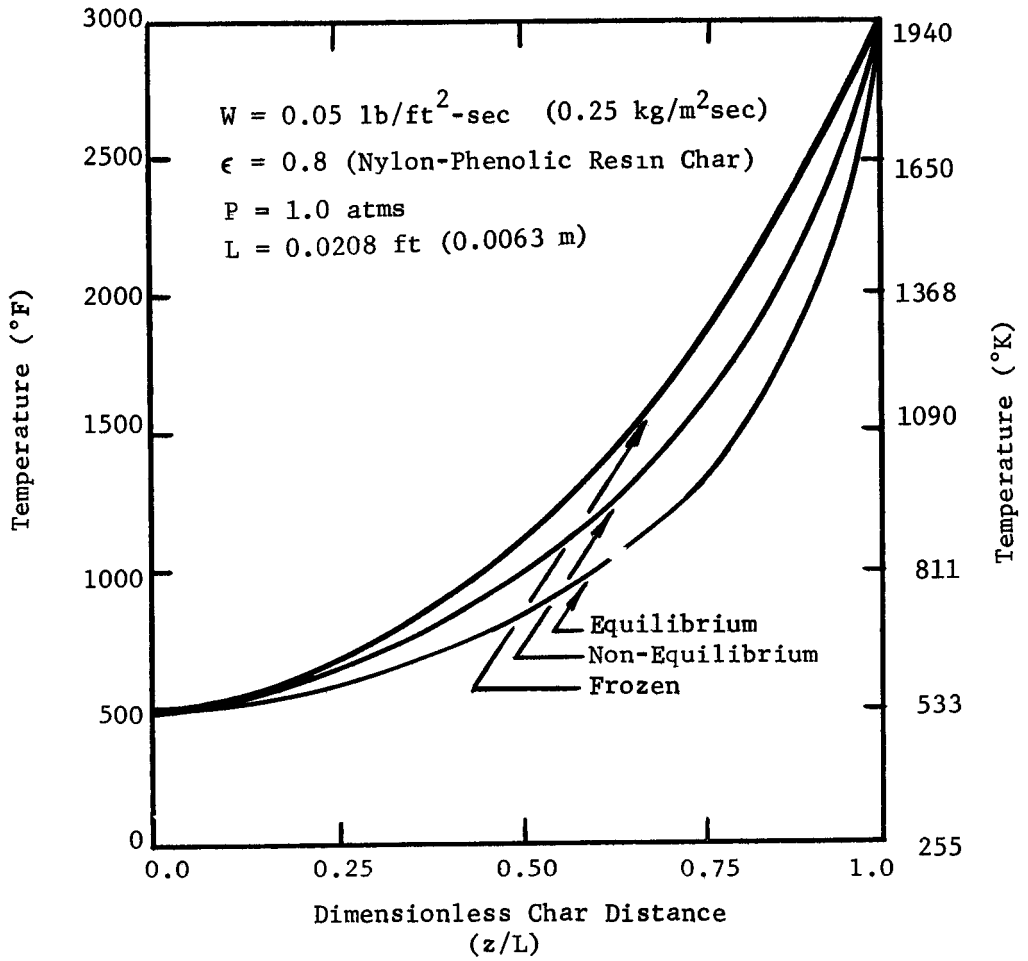

Figure 6. Temperature Profile for the Frozen, Equilibrium, and Non-Equilibrium Flow of Pyrolysis Gases Through the Char Zone of a Nylon-Phenolic Resin Ablator.

Table 7. Results of the Frozen, Equilibrium and Nonequilibrium Flow Analyses for Pyrolysis Gas Flow Through a One-Quarter Inch Low Density Nylon-Phenolic Resin Char at 3000°F (1940°K) T_L.

Conditions: $W = 0.05$ lb/ft^{2}sec (0.25 kg/m^2-sec) $\epsilon = 0.8$, $L = 0.0208$ft (0.0063 m) $T_o = 500°F$ ($533°K$) $T_L = 3000°F$ ($1940°K$)

Char Position:	Inlet	Exit (z/L) = 1		
Flow Model	(All)	Frozen	Equilibrium	Nonequilibrium
Composition (Mole%):				
Hydrogen	33.4	33.4	80.0	0.0
Methane	6.7	6.7	0.0	54.0
Phenol	6.2	6.2	0.0	2.4
Water	48.9	48.9	0.2	0.0
Carbon Monoxide	3.7	3.7	10.4	28.9
Carbon Dioxide	1.1	1.1	9.4	17.4
Pressure Drop (lb/ft^2):	-	11.3	7.3	11.0
(kg/m^2)	-	56.5	36.5	55.0
Heat Flux (BTU/ft^{2}sec)	-	92.5	335.5	193.4
(KJ/m^2-sec)	-	1017.3	3690.5	2126.9

(a) Nonequilibrium flow model requires additional important reactions and associated kinetic data to accurately describe the energy transport above ~3000°F (1940°K).

where a value of 0.95 was used for the emissivity, . This information is summarized in Fig. 7 in which the mass flux is plotted against the approximate aerodynamic heating for various heats of pyrolysis, Q_p. The heat of pyrolysis is a function of the composition of the heat shield and is calculated by making an energy balance at the back surface of the char:

$$Q_p = -k_e \left.\frac{dT}{dz}\right|_{z=0} \tag{10}$$

where Q_p is the sum of the energy absorbed by the decomposition of the plastic heat shield and the energy conducted through the virgin plastic. Results for the frozen, equilibrium and nonequilibrium flow models are presented. This form of presenting the results is a very convenient and informative method as will be seen.

In heat shield design one of the important questions asked is, "What is the required heat shield weight necessary for the protection of a vehicle for a specific mission?". Specification of the type of heat shield material to be used (ė.g., nylon-phenolic resin) brackets the heat of pyrolysis value, while the trajectory calculations determine the amount of aerodynamic heating that can be expected. For example, an approximate aerodynamic heating rate of 500 BTU/ft^2-sec (5×10^6 J/m^2-sec) and a heat of pyrolysis of 400BTU/lb (8×10^5 J/kg) locates three distinctive points on Fig. 7; one for each of the frozen, equilibrium and nonequilibrium flow models. This corresponds to three values of the mass flux; 0.017 lb/ft^2-sec (0.085 kg/m^2-sec) for frozen, 0.002 lb/ft^2-sec (0.01 kg/m^2-sec) for equilibrium and 0.009 lb/ft^2-sec (0.045 kg/m^2-sec) for nonequilibrium flow. The nonequilibrium flow analysis accurately predicts the behavior and would specify the more correct heat shield weight (which is a function of the mass flux) required. The frozen flow model shows an overprediction because important endothermic chemical reactions are omitted, and the equilibrium flow model shows an underprediction because chemical reactions are assumed to

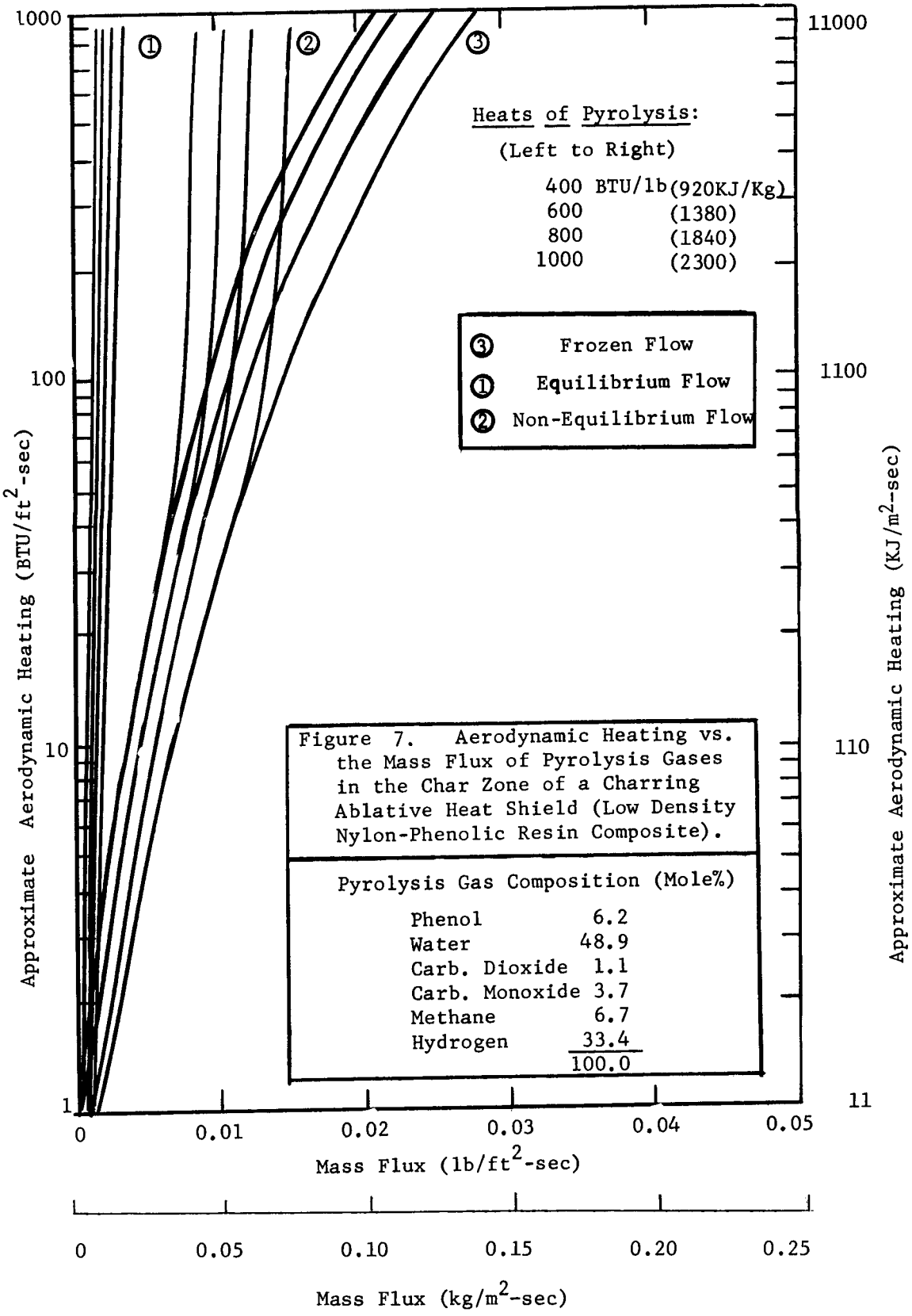

Figure 7. Aerodynamic Heating vs. the Mass Flux of Pyrolysis Gases in the Char Zone of a Charring Ablative Heat Shield (Low Density Nylon-Phenolic Resin Composite).

Pyrolysis Gas Composition (Mole%)	
Phenol	6.2
Water	48.9
Carb. Dioxide	1.1
Carb. Monoxide	3.7
Methane	6.7
Hydrogen	33.4
	100.0

occur at a greater extent than the actual behavior.

The results presented in Fig. 7 also provide a method determining at what point the nonequilibrium flow changes from frozen flow behavior. Referring to the figure all three models give the same result only at very low mass fluxes and approximate aerodynamic heating. The break between non-equilibrium and frozen flow occurs about a mass flux of 0.01 lb/ft^2-sec (0.05 kg/m^2-sec).

Calculation of the Reacting Gas Heat Capacity

In addition to the above information, the reacting gas heat capacity for the nonequilibrium flow of pyrolysis products through a porous char layer has been determined. This term is very useful in the calculations of the one-dimensional, transient response of an ablative composite structure. The energy equation for the transient case can be put in the following form for the char zone:

$$-\frac{\partial}{\partial z}\left(k\frac{\partial T}{\partial z}\right) + \left[\left(\frac{W}{W_o}\right)\bar{C}_p + \frac{\sum_{i=1}^{k+1} H_i R_i}{W_o\left(\frac{\partial T}{\partial z}\right)}\right] W_o \frac{\partial T}{\partial z} = -C_p \frac{\partial T}{\partial z} \qquad (11)$$

where W is the mass flux of pyrolysis products at z, and W_o is the mass flux of pyrolysis products entering the char. The term in brackets is referred to as the reacting gas heat capacity. In Fig. 8 a plot of the reacting gas heat capacity as a function of temperature is shown for frozen, equilibrium and nonequilibrium flow within the char layer up to 3000°F (1925°K). These curves were calculated for a mass flux of 0.05 lb/ft^2-sec (0.25 kg/m^2-sec), a back surface temperature of 500°F (533°K), and, char porostiy and thickness of 0.8 and 0.25 inches (0.0063m), respectively. The differences in the method used to calculate the energy transfer by chemical reaction (H_iR_i) for equilibrium and non-equilibrium flow causes the curves to separate as shown at the highest temperature.

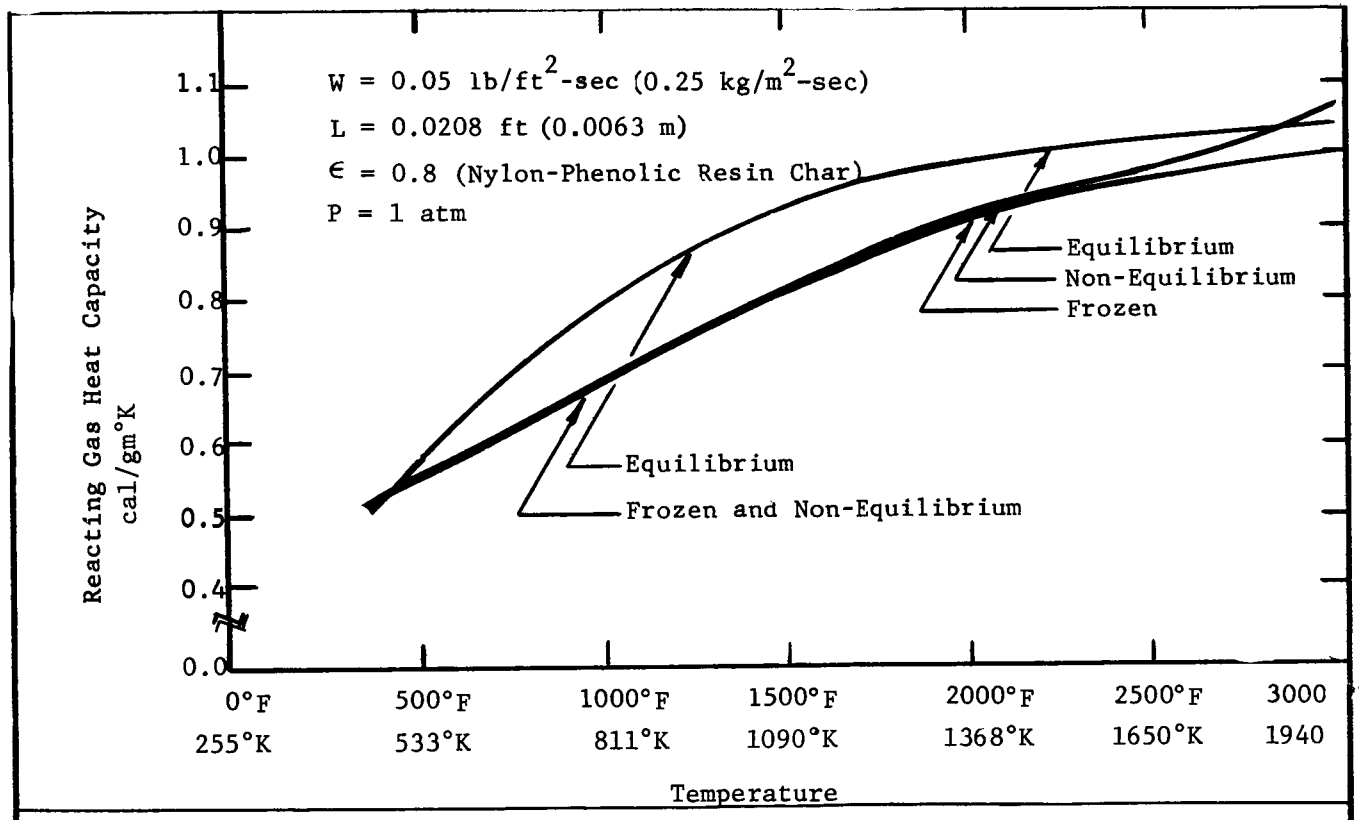

Figure 8. Plot of the Reacting Gas Heat Capacity for Frozen, Equilibrium and Non-Equilibrium Flow of Pyrolysis Gases Through the Char Zone.

Flow of Pyrolysis Products Through Chars and Porous Graphite

There are two important reasons for using porous graphite to simulate low density, nylon-phenolic chars used in ablative heat shield applications. These are availability and machinability of the graphite.

Nylon-phenolic resin chars were obtained from the National Aeronautics and Space Administration's Langley Research Center for use in the Char Zone Thermal Environment Simulator. Electric air-arc jets were used to char the nylon-phenolic resins, and this represented a considerable effort in supplying just a few specimens for use in this research. Although two sections of char were usually obtained from each specimen, the demand for additional chars could not be readily met. In addition to the problem of obtaining the samples, the brittle nature of the chars caused serious problems in mounting on the char holder section. These complications led to the testing and use of graphite, especially, for use in radioactive tracer and catalyst evaluation studied. However, for the successful substitution of graphite for the chars to be complete, the chemical behavior of the two must be essentially the same. Specifically the reactions and rates occurring in the char must be the same as those in porous graphite. This will be shown in the following sections by comparing the exit gas compositions from the Char Zone Thermal Environment Simulator with the composition predicted by the nonequilibrium flow model, and by direct comparison of char and graphite experimental results over a range of mass flux rates and front surface temperature common to both.

Other than the differences in the structural properties of chars and graphite, the one most important consideration that must be accounted for is the change in mass flux rates caused by differences in material porosity. Therefore, to put the materials on a common basis the mass flux rates previously discussed

in terms of the total area (kg/m^2total-sec) must be divided by the porosity to obtain rates within the pores (kg/m^2voids-sec). Even though the superficial mass flux rates are different for each porous medium, the mass flux rate within the pores will be the same. Again, the porosity of the chars and graphite were 0.8 and 0.5, respectively.

The foregoing discussion is not intended to mean that chemical reactions will not be influenced by other structural properties beside the porosity (e.g., crystallicity, permeability, etc.). However, it emphasizes that the mass flux within the pore spaces must be equivalent for a valid comparison. Differences in the chemical reaction rates resulting from differences in structural makeup could eliminate graphite as a suitable substitute. However, this could only be determined by a comparison of experiments conducted over the range of conditions for which the proposed flow model is valid.

In Table 8 the exit gas composition from the Char Zone Thermal Environment Simulator for the flow of pyrolysis products through graphite are presented for mass flux rates of 0.0034 to 0.0059 lb/ft^2-sec (0.017-0.30 kg/m^2-sec) at a front surface temperature of approximately 1950°F (1340°K). As in the case with chars, there is a significant amount of chemical reactions occuring in the porous medium for the lower mass flux (0.05 kg/m^2-sec). More importantly, however, it is the agreement, within experiment error, between the measured exit gas compositions and the predicted values by the non-equilibrium flow model using the same kinetic data employed for the char experiments.

A similar comparison if presented in Table 9 for an average mass flux rate of 0.0035 lb/ft^2-sec (0.017 kg/m^2-sec) and front surface temperatures of 1950°F (1340°K) and 2065°F (1410°K). Again, agreement within the experimental accuracy of the analyses was obtained between the non-equilibrium flow model

Table 8. Flow of Pyrolysis Gases Through Graphite. Effect of Changing Mass Flux Rates at a Front Surface Temperature of 1950°F (1340°K)

RUN NUMBER MASS FLUX FRONT TEMP BACK TEMP	FLOW MODEL	H_2 MOLE %	CH_4 MOLE %	CO MOLE %	CO_2 MOLE %	N_2 MOLE %	H_2O MOLE %	C_6H_6O MOLE %	C_2H_4 MOLE %	C_2H_2 MOLE %	MODEL	
											ΔP	q_{cz}
XXVIII-93	FROZEN	25.8	7.2	4.3	1.3	0.0	50.1	11.3	0.0	0.0	0.2	1.92
0.0170	EQUILIBRIUM	62.7	1.3	33.5	0 8	0.0	1.7	0.0	0.0	0.0	0.2	28.4
1340°K	NON-EQUILIBRIUM	32.8	10.0	11.8	4.1	0.0	32.6	10.2	0.0	0.3	0.2	2.33
860°K	EXPERIMENTAL	32.2	11.2	9.2	4.0	0.0	33.2	9.8	0.2	0.2	0.3	-
XXVIII-92	FROZEN	27.5	5.3	3.1	1.0	0.0	52.5	10.6	0.0	0.0	0.3	2.44
0.0220	EQUILIBRIUM	62.5	1.2	33.9	0.8	0.0	1.6	0.0	0.0	0.0	0.3	35.48
1320°K	NON-EQUILIBRIUM	29.3	7.7	8.0	2.5	0.0	42.2	10.1	0.0	0.2	0.3	2.75
866°K	EXPERIMENTAL	30.0	8.7	8.0	3.4	0.0	39.9	9.6	0.2	0.2	0.4	-
XXIX-95	FROZEN	21.7	4.6	2.8	0.8	0.0	57.1	13.1	0.0	0.0	0.5	7.34
0.0295	EQUILIBRIUM	61.1	1.4	34.0	1.3	0.0	2.2	0.0	0.0	0.0	0.3	25.8
1325°K	NON-EQUILIBRIUM	22.9	5.1	4.7	1.2	0.0	53.1	12.9	0.0	0.1	0.5	7.65
780°K	EXPERIMENTAL	21.9	6.6	5.4	2.1	0.0	52.0	11.3	0.3	0.4	0.4	-

Table 9. Flow of Pyrolysis Gases Through Graphite. Effect of Changing the Front Surface Temperature at a Mass Flux Rate of 0.0160 Kg/m^2-sec

RUN NUMBER MASS FLUX FRONT TEMP BACK TEMP	FLOW MODEL	H_2 MOLE %	CH_4 MOLE %	CO MOLE %	CO_2 MOLE %	N_2 MOLE %	H_2O MOLE %	C_6H_6O MOLE %	C_2H_4 MOLE %	C_2H_2 MOLE %	MODEL	
											ΔP	q_{cz}
XXVIII-93	FROZEN	25.8	7.2	4.3	1.3	0.0	50.1	11.3	0.0	0.0	0.2	1.92
0.0170	EQUILIBRIUM	62.7	1.3	33.5	0.8	0.0	1.7	0.0	0.0	0.0	0.2	28.4
1340°K	NON-EQUILIBRIUM	30.8	10.0	11.8	4.1	0.0	32.6	10.2	0.0	0.3	0.2	2.33
860°K	EXPERIMENTAL	32.2	11.2	9.2	4.0	0.0	33.2	7.8	0.2	0.2	0.3	-
XXIII-71	FROZEN	25.8	4.9	2.9	0.9	0.0	54.7	10.8	0.0	0.0	0.2	2.02
0.0155	EQUILIBRIUM	62.6	0.7	35.8	0.3	0.0	0.7	0.0	0.0	0.0	0.2	31.85
1400°K	NON-EQUILIBRIUM	41.4	8.4	23.9	5.1	0.0	12.5	8.2	0.0	0.6	0.2	3.23
858°K	EXPERIMENTAL	39.3	8.8	27.2	5.9	0.0	11.2	7.6	0.0	0.0	0.7	-

the experimental accuracy of the analyses was obtained between the non-equilibrium flow model compositions and the experimental values.

As a final comparison, several char and graphite experiments are examined in Table 10. To accomplish this the mass flux rates based on the void area were calculated and are shown in brackets. The listing in Table 10 is, also, made in order of increasing chemical reactions; i.e., low temperatures and high mass flux rates appear first. As seen, the char and graphite experiments are indeed compatible and behave in essence as one material. Consequently, this permits the use of the more easily workable graphite materials in experiments designed to study carbon deposition and product distribution using carbon-14 tracers, and, to investigate the effect of catalysts in accelerating the rates of chemical reactions within the char layer. Details of the results from these experimental investigations follow.

Radioactive Tracer Studies Using Porous Graphite

Radioactive methane and phenol in simulated pyrolysis products were used in separate experiments to determine the specific products of decomposition from each labeled species. Also, the amount and location of carbon deposition in the char due to the thermal cracking of each species was determined.

The method used involved the sampling of the exit simulated pyrolysis products stream followed by gas chromatographic analysis. The fractionated gas chromatographic effluent stream was then passed through a combustion furnace forming carbon dioxide and water. After trapping the water, the carbon dioxide was absorbed in a one molar hydroxide of hyamine (in methanol) solution. Collecting the radioactive concentrations corresponding to the separated gases indicated on the gas chromatogram. By comparing the two curves for identical retention times, the relative amount of each carbon-containing species formed from the thermal degradation of the labeled pyrolysis product entering the char was determined.

Table 10. Flow of Pyrolysis Gases Through Graphite and Chars. Comparison of Results.

RUN NUMBER MASS FLUX: W (W_p) FRONT TEMP BACK TEMP	FLOW MODEL	H_2 MOLE %	CH_4 MOLE %	CO MOLE %	CO_2 MOLE %	N_2 MOLE %	H_2O MOLE %	C_6H_6O MOLE %	C_2H_4 MOLE %	C_2H_2 MOLE %	MODEL	
											ΔP	q_{cz}
C-XVIII-56	FROZEN	28.9	6.4	3.3	0.8	0.0	53.3	6.9	0.0	0.0	0.4	0.93
0.01040	EQUILIBRIUM	59.7	3.3	26.7	4.0	0.0	6.3	0.0	0.0	0.0	0.4	15.93
(0.01300)	NON-EQUILIBRIUM	23.0	11.1	2.8	2.1	0.0	53.8	7.1	0.0	0.0	0.4	0.99
1190°K	EXPERIMENTAL	24.8	10.3	3.4	1.3	0.0	53.7	6.5	0.0	0.0	0.8	-
820°K												
G-XXVIII-93	FROZEN	25.8	7.2	4.3	1.3	0.0	50.1	11.3	0.0	0.0	0.2	1.92
0.0170	EQUILIBRIUM	62.7	1.3	33.5	0.8	0.0	1.7	0.0	0.0	0.0	0.2	28.40
(0.0340)	NON-EQUILIBRIUM	28.8	10.0	11.8	4.1	0.0	32.6	10.2	0.0	0.3	0.2	2.33
1340°K	EXPERIMENTAL	32.2	11.2	9.2	4.0	0.0	33.2	9.8	0.2	0.2	0.4	-
865°K												
C-XIX-60	FROZEN	29.3	6.0	3.3	0.9	0.0	53.7	6.8	0.0	0.0	0.7	1.17
0.01240	EQUILIBRIUM	62.7	0.8	35.2	1.5	0.0	0.9	0.0	0.0	0.0	0.6	13.00
(0.01550)	NON-EQUILIBRIUM	38.2	17.2	25.2	8.8	0.0	4.9	5.1	0.0	0.5	0.6	2.42
1370°K	EXPERIMENTAL	41.3	18.2	23.4	7.6	0.0	5.0	4.5	0.0	0.0	0.6	-
1020°K												
G-XXIII-71	FROZEN	25.8	4.9	2.9	0.9	0.0	54.7	10.8	0.0	0.0	0.2	2.02
0.01550	EQUILIBRIUM	62.6	0.7	35.8	0.3	0.0	0.7	0.0	0.0	0.0	0.2	31.85
(0.03100)	NON-EQUILIBRIUM	41.4	8.4	23.9	5.1	0.0	12.5	8.2	0.0	0.6	0.2	3.23
1380°K	EXPERIMENTAL	39.3	8.8	27.2	5.9	0.0	11.2	7.6	0.2	0.3	0.7	-
865°K												
C-XX-63	FROZEN	28.6	5.5	3.4	1.0	0.0	53.8	7.7	0.0	0.0	0.6	1.79
0.01120	EQUILIBRIUM	63.1	0.3	36.4	0.1	0.0	0.2	0.0	0.0	0.0	0.5	51.37
(0.01400)	NON-EQUILIBRIUM	30.7	21.4	38.6	3.4	0.0	0.0	4.6	0.3	1.0	0.5	3.18
1535°K	EXPERIMANTAL	30.4	19.8	38.0	5.7	0.0	0.0	5.0	0.5	0.6	0.6	-
905°K												

Typical results for the simulated pyrolysis products containing carbon-14 labeled methane are shown in Figure 9, in which the gas chromatograms and corresponding radioactivity curve are presented. In this experiment the front surface temperature was 1935°F (1333°K) and the gas mass flux was 0.0059 lb/ft^2-sec (0.030 kg/m^2-sec). By comparing the two curves, the products of methane decomposition were found to be unreacted methane, carbon monoxide, carbon dioxide, ethylene and acetylene. These results for methane are very important in the light of predicting the manner in which energy can be absorbed by chemical reaction. Ethylene and acetylene, for example, are indirect products of methane decomposition predicted by reactions (2), through (3) in Table 1, while carbon monoxide and dioxide are formed by the reaction of steam with deposited carbon in reactions (8) through (10). This information assisted in establishing that the chemical reactions used in the analysis are correct.

A similar discussion is presented for simulated pyrolysis products containing labeled phenol. These results are likewise shown in Figure 9. Conditions for the presented data were a front surface temperature of 1960°F (1350°K) and a mass flux rate of 0.0034 lb/ft^2-sec (0.017 kg/m^2-sec). The exit gas products for phenol degradation were methane, carbon monoxide, carbon dioxide, ethylene and acetylene, as well as unreacted phenol analysed in the liquid phase. Once again insight into the kind of reactions necessary to product the products was obtained. The formation of hydrogen and carbon by reaction (6), (7), and (4) is probably by the observed carbon deposition within the graphite. Hydrogenation of carbon by reaction (5) to form methane, followed by the steam-gas reactions (8,9,10) and the hydrocarbon cracking reactions (1,2,3,4) accounts for each readioactive species observed.

In both methane and phenol degradation, thermal decomposition of the major

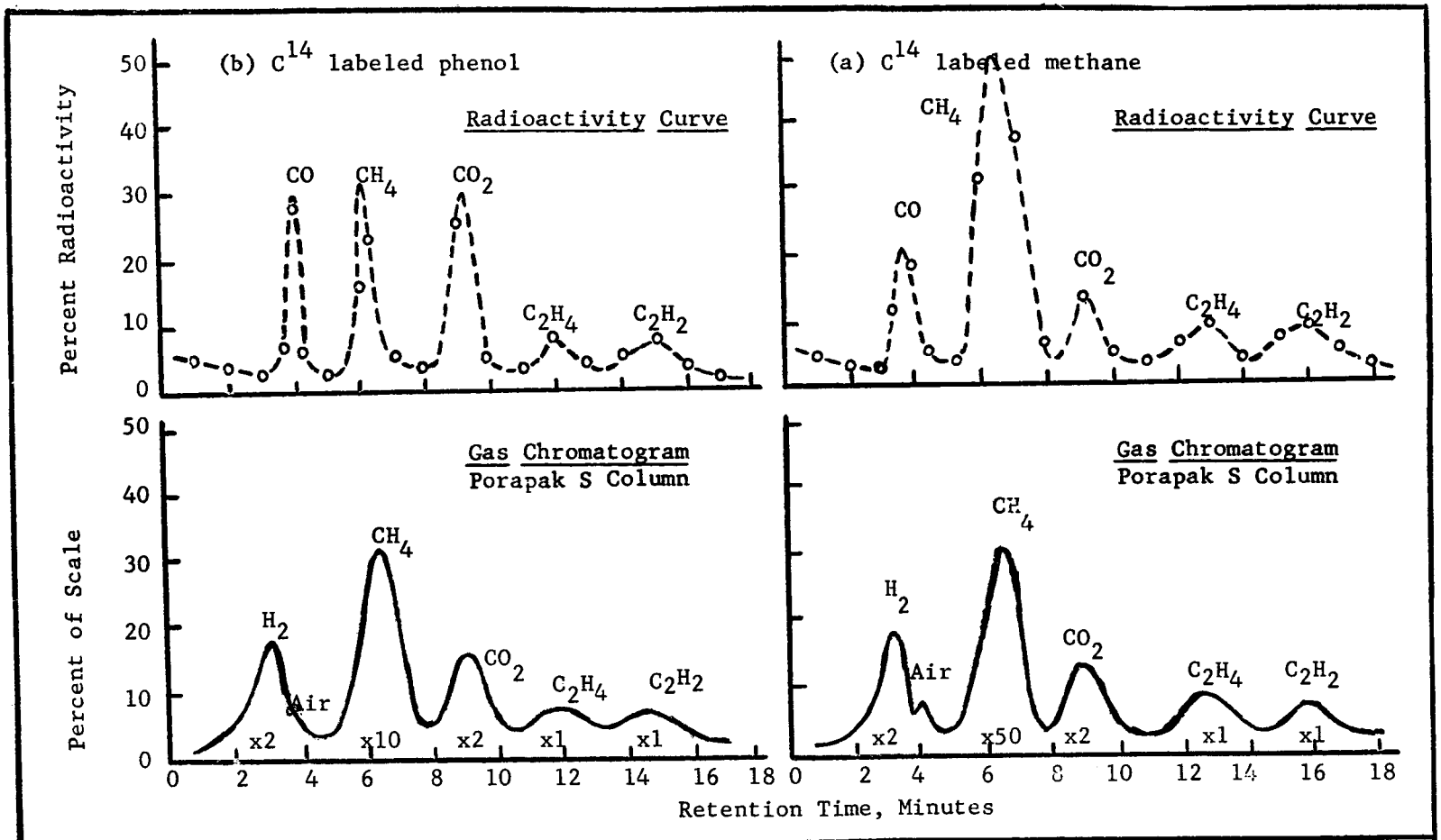

Figure 9. Gas Chromatograms and Radioactivity Curves of the Exit Product Stream from the Char Zone Thermal Environment Simulator; (a) C^{14} labeled methane, (b) phenol.

species in the simulated pyrolysis product steam was described and accounted for by the reactions considered important between 500-3000°F (533-1925°K). In addition to the product distribution resulting from the thermal degradation of methane and phenol, deposited carbon was also observed to occur. The location of the carbon deposition within the char layer is important in defining the temperature at which reactions become significant. This topic is discussed in detail in the next section.

Carbon Deposition Studies by Radioactive Tracer Methods

The location and extent of carbon deposition resulting from methane and phenol decomposition was determined using carbon-14 labeled methane and phenol. In the specific cases studied, labeled methane and phenol were fed separately as components in the simulated pyrolysis product steam entering the char. The char was removed after each experiment and sectioned by removing thin layers using emery paper. These layers varied between one and ten percent (by weight) of the total char and were combusted separately with collection of the carbon dioxide in one molar hydroxide hyamine (in methanol) solution. The radioactivity of each thin layer was determined and plotted as a function of char depth. In Figure 10 such a curve is shown for the thermal degradation of phenol and Figure 11 is a similar curve for the decomposition of radioactive labeled methane. The hashed-in rectangular blocks represent the total percent radioactivity of the thickness of the individual slices analysed, while the dotted curve represents the percent radioactivity per unit thickness at a particular char depth. The results in Figure 10 are for phenol decomposition at a mass flux rate of 0.0059 lb/ft^2-sec (0.030 kg/m^2-sec) and a front surface temperature of 1960°F (1350°K). Deposition of carbon appears to start at a char depth of 0.38 corresponding to a temperature of 1300°F (978°K), and continues uniformly to 0.925 where the temperature is

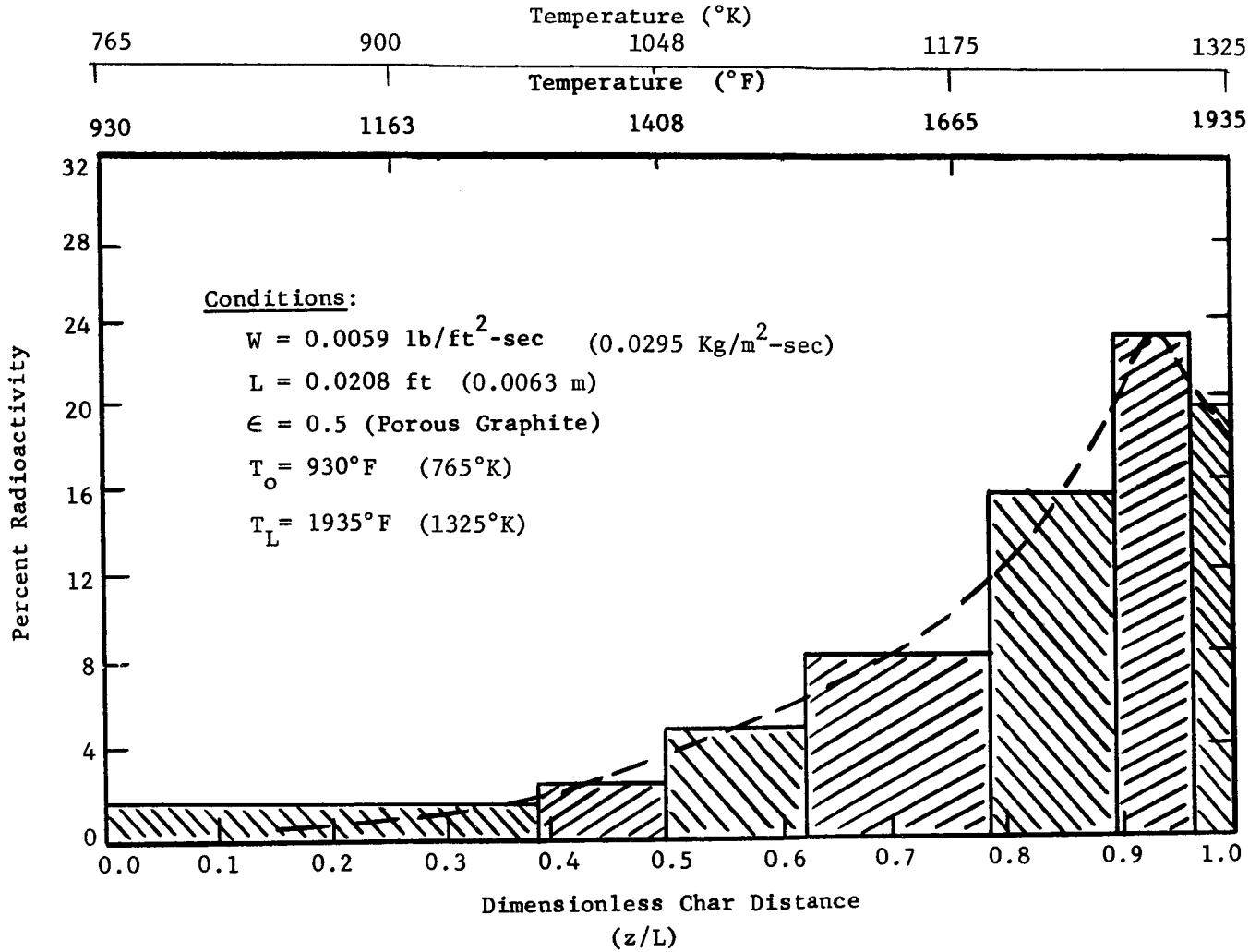

Figure 10. Carbon Deposition Profile for the Thermal Degradation of Phenol, a Major Component in the Pyrolysis Gas Stream.

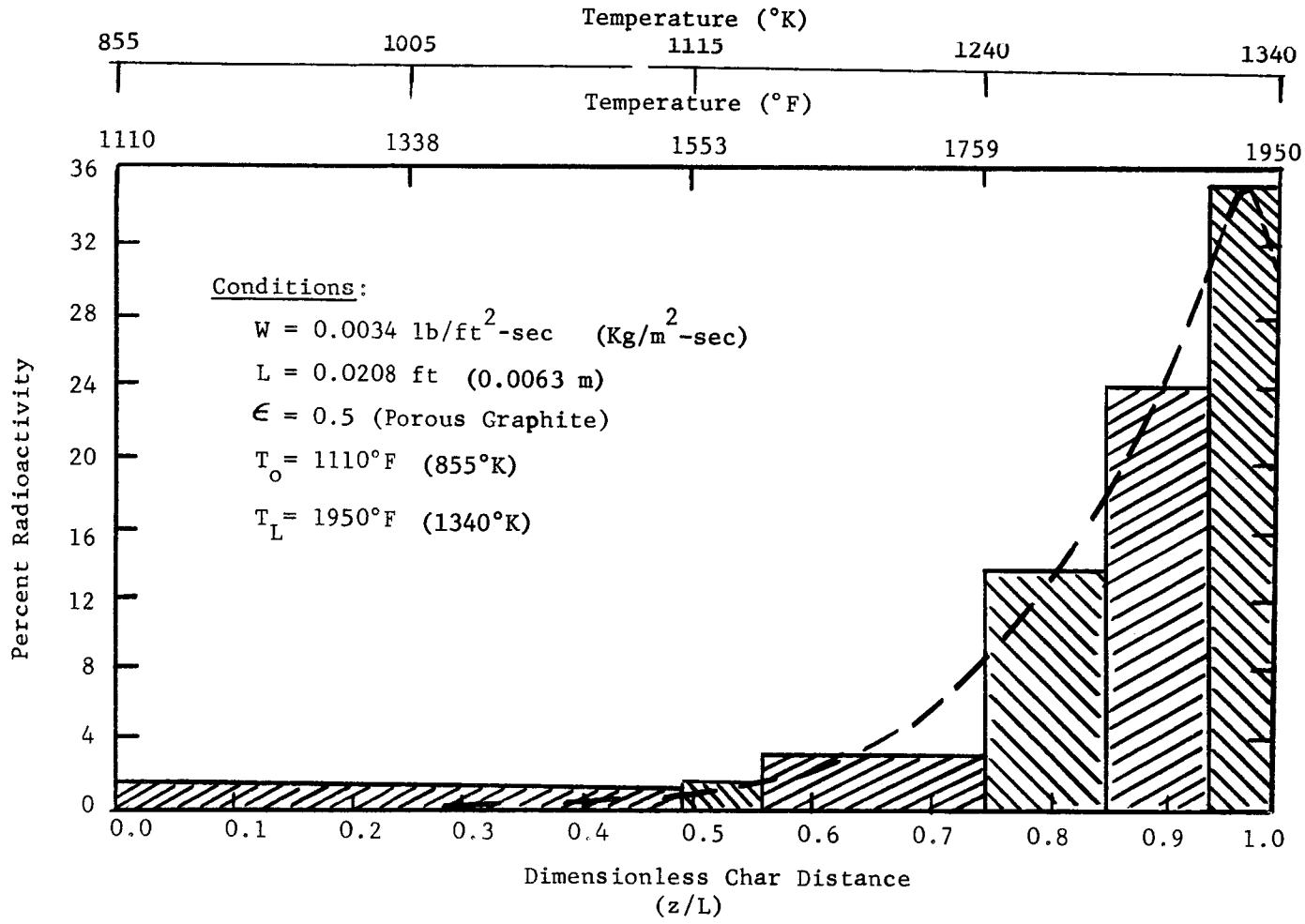

Figure 11. Carbon Deposition Profile for the Thermal Degradation of Methane, a Major Component in the Pyrolysis Gas Stream.

1925°F (1325°K). At this point a rapid decrease is noted indicating either no further carbon deposition or disappearance of carbon by chemical reaction.

Similar results are observed for carbon deposition by methane decomposition in Figure 11. Since methane and/or phenol was present in the exit gas stream, it is unlikely that carbon deposition reactions have terminated. Instead, the reaction of the deposited carbon with steam (or carbon dioxide) is a more probably explanation of the decline noted in Figure 11. This was also substantiated by the rapid decrease in water concentration at the same temperature where carbon deposition declines. Additionally, carbon was observed on the quartz cover plate and inside surfaces of the outer char holder section which indicated that the carbon deposition reactions were continuing after the gases had left the char surface.

In summary, a comprehensive picture of carbon deposition with regard to its location, the causes for its appearance and disappearance, and its effect on the exit gas product distribution was obtained. The combination of the radiative tracer techniques and the non-equilibrium flow analysis will be applied in evaluating various catalysts for accelerating the chemical reactions and, thereby, increasing the energy absorbed within the char zone. The effectiveness of each catalyst will be determined in the following section by comparing the results with data from non-catalytic experiments and the non-equilibrium flow model.

Catalytic Reactions of the Pyrolysis Products in the Char Zone

The discussion thus far has shown that chemical reactions within the char layer are very important for energy absorption. It was also pointed out that chemical non-equilibrium becomes important between 2000-2500°F (1367-1644°K) for a mass flux rate of 0.05 lb/ft^2-sec (0.25 kg/m^2-sec) (Tables 4 through 7). Below this range, the flow of pyrolysis products through the char is essentially frozen. In applications where the temperatue gradient across the ablator may vary from

500-5000°F (533-5033°K), the frozen state (less than 1367°K) can extend over nearly one third the entire thickness. Within this region heat absorption by conduction and convection are the only important modes of energy transfer. In order to increase the capacity of this region to absorb heat, and thus proportionately reduce the total heat shield weight, the introduction of catalysts to initiate chemical reactions in the lower temperature range (<1367°K) was evaluated.

There are two types of catalyst systems: homogeneous and heterogeneous. The first involves the introduction of a chemical compound which is in the same phase as the pyrolysis gases. The homogeneous catalyst effectively reduces the energy of activation by interacting with the various species present. To illustrate this interaction the catalytic chlorination of nitrous oxide in the presence of bromine is used as an example (Ref. 9) of the action of a homogeneous catalyst. The direct chlorination occurs by Reaction (12):

$$2NO + Cl_2 \rightarrow 2NOCl \tag{12}$$

Introducing the bromine results in a two reaction sequence as follows:

$$2NO + Br \rightarrow 2NOBr \tag{13}$$

$$2NOBr + Cl_2 \rightarrow 2NOCl + Br_2 \tag{14}$$

The reaction with the greatest activation energy between (13) and (14) is the rate determining step for the sequence. Bromine is considered a catalyst if, and only if, the energy of activation of the rate determining step is smaller than the energy of activation of reaction (12). Such is the case for this example. Other homogeneous catalysts are iodine, hydrogen bromine, hydrogen fluoride, nitric oxide, chlorine and mercury (10,11,12,13,14).

In the case of the halogens, incorporation of an organic halide into the composite whic thermally degrades at or near the temperature for the nylon-

phenolic resin composite could be used to introduce the catalyst into the pyrolysis products. One example for bromine is tribromobutane which vaporizes at 500°K (nylon-phenolic resin at 525°K) and forms HBr and cracked products of an olefin.

The second type of catalyst with application to flow of hydrocarbon products through porous media is the heterogeneous catalyst. These consist of a thin dispersion of an active metal on a porous solid, called a catalyst support. Fluids are thus absorbed on the metal surfaces as they flow through the porous solid, undergo chemical reactions, and desorb back into the gas stream. The kind of solid supports used vary from clays and alumina to porous carbon.

Heterogeneous catalysts are widely used in the petroleum and chemical industries for accelerating hydrogenation and dehydrogenation reactions, hydrocracking reactions and hydroforming reactions. Some typical active metals used in these applications are platinum, tungsten, molybdenum, palladium, etc. (15). One example involves the catalytic hydrogenation of benzene to cyclohexane at room temperature with platinum on porous carbon supports (15). Cyclohexane is then cracked to lower molecular weight compounds at 722°K (16). Details for the catalytic cracking of numerous organic compounds are presented by Vogh (17).

In many cases the use of heterogeneous catalysts is restricted to applications which do not contain compounds that deactivate the metal surfaces. Some of these so called poisons are carbon monoxide, sulfur and deposits of carbon or coke. Although there is no sulfur in the pyrolysis product stream, carbon monoxide and deposited carbon are present requiring additional screening of the heterogeneous catalyst considered. Because the heterogeneous catalyst is on the solid surface, there are two possible techniques for placement of a finely dispersed metal catalyst on the char surface during ablation. The first would employ a nylon-platinum catalyst used to hydrogenate benzene to cyclohexane (Ref.

18). This platinum impregnated nylon could be moulded with phenolic resin. During ablation, the nylon would degrade and release the metal catalyst which would be distributed on the char surface. The presence of water and hydrogen at the lower temperatures (750°K) would prevent coking, leaving the metal sites exposed to promote the pyrolysis reactions.

The second method is similar to the method used for introducing a homogenous catalyst into the pyrolysis product stream. In this case an organo-metallic compound such as nickel stearate (19) could be included which would vaporize in the decomposition zone with deposition of nickel on the char surface. This action is commonly observed in vapor phase cracking processes (19,20) in which increased activity of the cracking catalyst results in excessive carbon and hydrogen formation. Other similar compounds are the carbonyl compounds of nickel, iron and cobalt (21). The combination of both catalysts systems may also be possible by using compounds containing both metal and halogen atoms, such as platinum iodide. The advantage of this type of co-catalyst would exist only if both groups were found to accelerate chemical reactions within the char layer.

The following sections describes the results obtained in tests using the Char Zone Thermal Environment Simulator. Each catalyst system will be compared with non-catalytic data to determine the extent of chemical reaction due to the addition of the catalyst. The preparation of each catalyst and the procedure for introducing it into the experimental simulation will also be discussed.

Homogeneous Catalysis: Unlike the heterogeneous catalysis systems, very little information regarding the activity of various homogeneous catalyst systems is contained in the literature. One source, however, reported the relative activity of several organic halides and halogen catalysts for the catalytic degradation of hydrocarbons to carbon monoxide, carbon dioxide, organic acids, aldehydes and ketones (22). A list of the relative activities of these

catalysts is presented in Table 11 with iodine as a reference (relative activity of 100). No relative activities of nitrous oxide or mercury were found. Also hydrogen fluoride was omitted from the above list of relative activities.

Although some of the above may indeed by excellent homogeneous catalysts, certain aspects of the ablative process prohibit their use. For example, nitrous oxide, while exhibiting excellent catalytic activity for the thermal degradation of certain hydrocarbons requires a concentration too great to be practically included in the composite (10). Similarly, hydrogen fluoride and mercury are almost exclusively used as liquid phase catalysts (23.24). As a result, attention in this research was given to the halides which were not only reported as good catalysts in hydrocarbon decomposition and oxidation reactions (25), but were also required in sufficiently small concentrations to be feasible for ablative heat shield applications.

Experimental Results for Homogeneous Catalysis of the Pyrolysis Product Reactions with Bromine: Bromine was selected as a representative halide catalyst for the experimental study. It was convenient to dissolve bromine in the water and feed the resulting solution with phenol and the gaseous pyrolysis products. The concentration of bromine in the water solution was varied from 1.0 to 4.0% (by wt.).

The selection of bromine as a suitable and typical catalyst was based on evidence of strong aromatic ring attack, such as with phenol, to form tribromophenol at ambient conditions. In addition it has excellent oxidative properties in decomposing hydrocarbons such as propane to carbon monoxide, carbon dioxide and other organic acids, aldehydes and ketones (25). Furthermore, the formation of HBr from hydrogen and bromine occurs at moderate temperatures (475-575°K) by the following mechanism (26). This gives the additional catalytic benefit of

Table 11. Relative Activity of the Halogens and Organic Halides as Catalysts in the Thermal Degradation of Pyrolysis Gases

Conditions: Oxidation of Aldehydhes and Ketones at 700-800°K and One Atmosphere.

Component Name	Relative Efficiency
Iodine (Reference)	100
Isopropyl Iodide	70
Ethyl Iodide	40
Methyl Iodide	30
Hydrogen Bromide	20
Isopropyl Bromide	5
Ethyl Bromide	4
Dibromoacetylene	3
Chlorides	0

HBr being present.

$$
\begin{aligned}
Br_2 &\rightarrow Br + Br \\
Br + H_2 &\rightarrow HBr + H \\
H + Br_2 &\rightarrow HBr + Br \\
H + HBr &\rightarrow H_2 + Br \\
Br + Br &\rightarrow Br_2^* \\
Br_2^* &\rightarrow Br + Br
\end{aligned}
\qquad (15)
$$

The above mechanism is favored by low pressure and large surface area, both of which exist in the char zone during reentry. In addition selecting bromine established a reference to the remaining halide catalysts contained in Table 11.

Results of several experiments are shown in Table 12. The experimental exit gas compositions are no longer predicted by the non-equilibrium flow model within the experimental accuracy as observed for the non-catalytic experiments. Also the reactions are not at equilibrium as seen from the table.

The effect of bromine as a catalyst is best illustrated by comparing Experiment XXVIII-92, in which the mass flux was 0.0044 lb/ft^2-sec (0.022 kg/m^2-sec), the front surface temperature of 1920°F (1322°K) and no bromine, with Experiment XXV-81 (mass flux of 0.010 kg/m^2-sec, a front surface temperature of 1955°F (1370°K) and 4% (wt) bromine catalyst) in Table 13. The conditions are almost the same, and the extent of reaction is greater for the experiment with bromine present. The addition of bromine accelerated the chemical reactions as seen by the facts that significantly more of the water (17.6% rather than 25.4%) and phenol (7.2% rather than 9.5%) had been consumed than would have been if bromine had not been present. This is also seen by direct comparison of the experimental exit gas compositions from each of the similar experiments. A measured decrease in the water and phenol concentrations, with corresponding increases in methane, carbon monoxide, carbon dioxide, ethylene and acetylene are obtained in the bromine

Table 12. Flow of Pyrolysis Gases Through Graphite. Effect of Bromine Catalyst on the Exit Gas Compositions.

RUN NUMBER MASS FLUX FRONT TEMP BACK TEMP	FLOW MODEL	H_2 MOLE %	CH_4 MOLE %	CO MOLE %	CO_2 MOLE %	N_2 MOLE %	H_2O MOLE %	C_6H_6O MOLE %	C_2H_4 MOLE %	C_2H_2 MOLE %	CATALYSTS
XXV-82	FROZEN	36.9	7.2	4.2	1.3	0.0	42.3	8.1	0.0	0.0	Bromine
0.0325	EQUILIBRIUM	66.2	0.8	32.1	0.2	0.0	0.7	0.0	0.0	0.0	in Water
1380°K	NON-EQUILIBRIUM	40.6	9.7	14.1	2.7	0.0	25.2	7.3	0.0	0.0	4%
860°K	EXPERIMENTAL	41.6	11.8	18.9	3.4	0.0	16.4	7.1	0.3	0.5	(by weight)
XXVII-87	FROZEN	2.3	3.4	0.4	0.1	0.0	0.0	93.8	0.0	0.0	Bromine
0.0160	EQUILIBRIUM	73.7	1.5	24.1	0.3	0.0	0.4	0.0	0.0	0.0	in Water
1350°K	NON-EQUILIBRIUM	2.8	3.6	0.5	0.1	0.0	0.0	91.3	0.0	0.6	1%
845°K	EXPERIMENTAL	4.8	2.7	0.8	0.1	0.0	0.0	90.2	0.1	0.3	(by weight)
XXVII-89	FROZEN	2.1	3.2	0.4	0.1	0.0	94.2	0.0	0.0	0.0	Bromine
0.0254	EQUILIBRIUM	51.1	0.6	46.7	0.7	0.0	1.0	0.0	0.0	0.0	in Water
1365°K	NON-EQUILIBRIUM	18.3	2.8	13.3	2.0	0.0	63.6	0.0	0.0	0.0	1%
850°K	EXPERIMENTAL	28.2	3.4	21.5	6.0	0.0	40.8	0.0	0.4	0.5	(by weight)
XXVI-84	FROZEN	34.3	6.6	3.9	1.1	0.0	45.4	8.7	0.0	0.0	Bromine
0.0065	EQUILIBRIUM	65.0	1.0	32.5	0.4	0.0	1.0	0.0	0.0	0.0	in Water
1370°K	NON-EQUILIBRIUM	39.5	10.7	16.6	3.8	0.0	21.5	7.5	0.0	0.4	2%
755°K	EXPERIMENTAL	37.8	15.3	21.0	4.8	0.0	14.2	6.3	0.2	0.4	(by weight)

Table 13. Flow of Pyrolysis Gases Through Graphite. Comparison of Bromine Catalyzed and Non-Catalytic Exit Gas Compositions.

RUN NUMBER MASS FLUX FRONT TEMP BACK TEMP	FLOW MODEL	H_2 MOLE %	CH_4 MOLE %	CO MOLE %	CO_2 MOLE %	N_2 MOLE %	H_2O MOLE %	C_6H_6O MOLE %	C_2H_4 MOLE %	C_2H_2 MOLE %	COMMENTS
XXV-81 0.0190 1350°K 903°K	FROZEN EQUILIBRIUM NON-EQUILIBRIUM EXPERIMENTAL	31.5 64.7 36.4 40.2	6.1 0.9 9.9 11.9	3.5 33.2 14.6 15.1	1.1 0.4 3.7 7.0	0.0 0.0 0.0 0.0	47.1 0.9 25.4 17.6	10.8 0.0 9.5 7.2	0.0 0.0 0.0 0.3	0.0 0.0 0.4 0.7	Bromine in Water 4% (by weight)
XXVIII-92 0.0220 1320°K 855°K	FROZEN EQUILIBRIUM NON-EQUILIBRIUM EXPERIMENTAL	27.5 62.5 29.3 30.0	5.3 1.2 7.7 8.7	3.1 33.9 8.6 8.0	1.0 0.8 2.5 3.4	0.0 0.0 0.0 0.0	52.5 1.6 42.2 39.9	10.6 0.0 10.1 9.6	0.0 0.0 0.0 0.2	0.0 0.0 0.2 0.2	No Bromine

catalysed experiment. These same trends are observed in all investigations with bromine and are independent of the catalyst concentrations used (1.0 to 4.0% by weight).

The effect of the bromine catalysis is also seen by inspecting the carbon deposition profiles for the thermal decomposition profiles of phenol in the simulated pyrolysis product stream. This is presented in Figures 12 and 13. The carbon deposition profile for the non-catalytic experiment is shown in Figure 12 for a mass flux of 0.0059 lb/ft^2-sec (0.030 kg/m^2-sec) and 1935°F (1330°K). Deposition begins at a distance of 0.38 in the char where the temperature is 1312°F (980°K) with a uniform increase to a maximum value at 0.925 or 1915°F (1320°K). At this point the profile decreases. In contrast to this curve, Figure 13 represents the carbon deposition profile for the bromine catalysed experiment in which the mass flux was 0.0075 lb/ft^2-sec (0.038 kg/m^2-sec) and 1900°F (1315°K). There is a definite shift in the carbon deposition curve with the maximum value moving from 0.925 to 0.71. Also additional carbon deposition was noted near the front surface at a temperature of about 1925°F (1325°K).

Similar profiles were obtained for carbon-14 labeled methane decomposition (Ref. 4). Although the results were not quite as pronounced as the phenol data, a detectable shift in the carbon deposition pattern was again observed. Deposition began at 0.48 (1120°K) for the non-catalytic experiment compared with 0.42 (1090°K) for the bromine catalyzed case. The point of maximum deposition was shifted awav from the front surface to a position corresponding to 1893°F (1300°K) or 0.85. The peak for the bromine-free experiment was located at 0.98 (1330°K).

In summary, these results showed that bromine is an active catalyst for the catalytic cracking of phenol in the presence of hydrogen (hydrocracking) and to a lesser extent for the hydrocracking of methane. A similar discussion regarding the cracking of the pyrolysis products using heterogeneous catalyst is presented

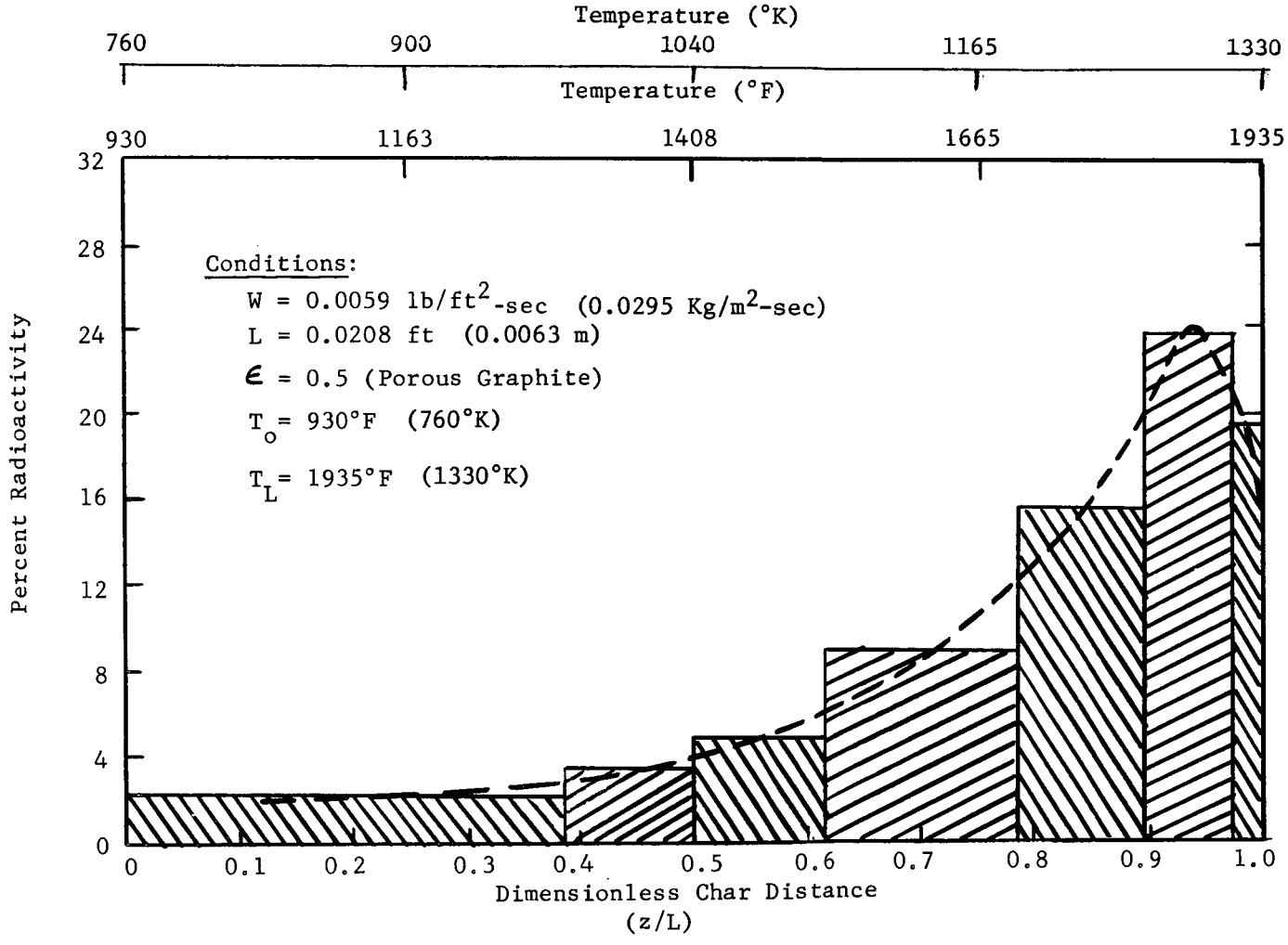

Figure 12. Carbon Deposition Profile for the Thermal Decomposition of Phenol, a Major Component in the Pyrolysis Gas Stream.

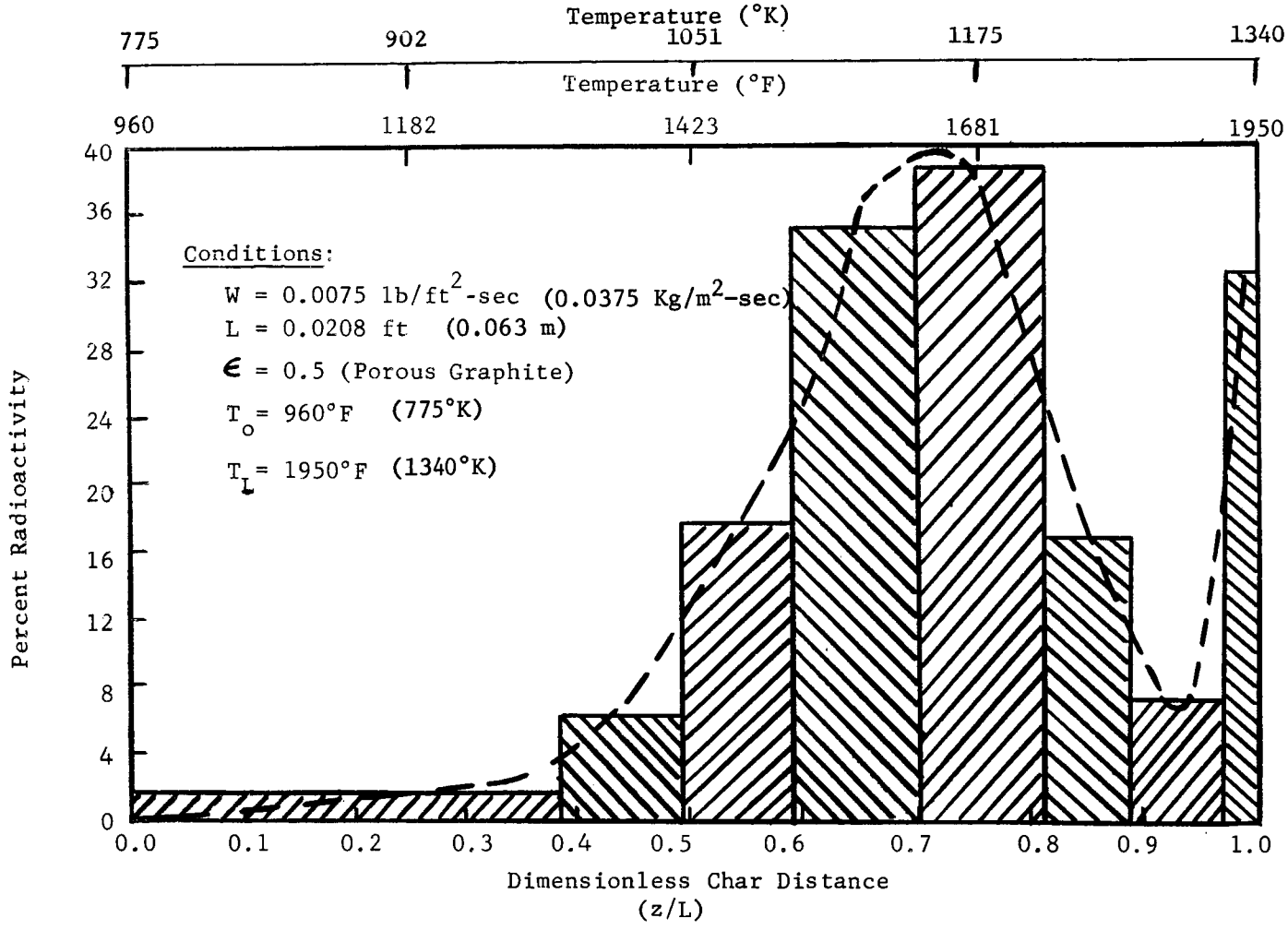

Figure 13. Carbon Deposition Profile for the Thermal Degradation of Phenol Catalyzed by Bromine in a Concentration of 4% (by weight).

in the following section.

Heterogeneous Catalysis of the Pyrolysis Product Reactions using a Tungsten-Molybdenum Co-Catalyst: A great deal of research into heterogeneous catalysts, their applications and activities has been reported in the literature (15,16,17,18). These catalysts are excellent hydrogeneration accelerators for a number of hydrocarbons common to the petroleum and chemical industries. However, they are also susceptible to deactivation by reaction, absorption or coating by several poisons. The two poisons which are present in the pyrolysis gases are carbon monoxide and coke (or carbon) formation. These two poisons are present in the char zone and must be considered when selecting possible heterogeneous catalysts. These poisons rule out the use of platinum, paladium, rhodium, nickel and selenium since these are all poisoned by carbon monoxide. In light of this discussion, tungsten, because of its relatively good activity in systems containing carbon monoxide, and molybdenum, because of its high selectivity in the thermal degradation of hydrocarbons, were selected as co-catalysts.

The method used to disperse these metals on the graphite specimens was the standard procedure to prepare heterogeneous catalysts and is as follows. First, the metals, as metal acids (anhydrous), were added to hot (353°K) sulfuric acid. Molybdenum was completely dissolved while tungsten formed a saturated solution. The graphite specimens were placed in the hot solution and stirred vigorously for thirty minutes. The second phase of the procedure involved the passing of carbon disulfide vapors through the graphite to convert the metal oxides to sulfides which increases the catalytic activity of the metals. The specimens were then dried at 316°K and reweighed to determine the weight of catalyst dispersed within the pores. The catalyst concentration varied from 5 to 6 percent (by weight) of the co-catalyst (50:50). This is typical of the dispersed (metal) phase composition of heterogeneous catalysts.

The effect of this catalyst on the reactions of the pyrolysis products in

the char zone is shown in Table 14. There are noticeable differences between the experimentally measured gas compositions and the computed values for the uncatalyzed case. However, they are not as pronounced as the results for bromine. This is better indicated by comparing the results of non-catalytic Experiments (XXVIII-92 and XXIX-94) with the values obtained in the heterogeneous co-catalyst systems (XXXII-92 and XXXI-98). The exit gas compositions are shown in Table 15 for an average mass flux rate of 0.0048 lb/ft^2-sec (0.025 kg/m^2-sec) and a front surface temperature range of 1860° to 1945°F (1260°K to 1336°K). No detectible difference between the four experiments is determined. Similarly, a comparison of the carbon deposition profiles for carbon-14 labeled phenol (XXVIII and XXXII) and methane (XXIX and XXXI) showed no substantial shift in the position of the maximum deposition or the location where carbon deposition begins. A slight difference in behavior near the front surface was observed but this represents no substantial change from the non-catalytic behavior.

A series of experiments with a platinum catalyst dispersed on the graphite specimens was also conducted using phenol-water free pyrolysis gases having a relatively low carbon monoxide concentration. These studies showed no catalytic activity over a temperature range of 1370° to 1755°F (1015°K to 1230°K). The flow remained frozen in each experiment studied.

Summary of the Catalytic Studies to Increase Reactions in the Char Zone: Results for adding bromine to the pyrolysis product stream as a homogeneous catalyst indicated increased chemical reactions within the char zone. This acceleration was shown by comparison of the exit gas composition based on the non-equilibrium (non-catalysed) flow model. Furthermore, carbon deposition profiles were used to locate the position and temperature where deposition resulting from methane and phenol thermal degradation occurred.

Table 14. Flow of Pyrolysis Gases Through Graphite. Effect of Molybdenum-Tungsten Co-catalyst on the Exit Gas Composition.

RUN NUMBER MASS FLUX FRONT TEMP BACK TEMP	FLOW MODEL	H_2 MOLE %	CH_4 MOLE %	CO MOLE %	CO_2 MOLE %	N_2 MOLE %	H_2O MOLE %	C_6H_6O MOLE %	C_2H_4 MOLE %	C_2H_2 MOLE %	CATALYST
XXXI-97 0.0320 1300°K 740°K	FROZEN EQUILIBRIUM NON-EQUILIBRIUM EXPERIMENTAL	20.0 59.4 20.4 21.6	4.2 1.7 4.6 5.6	2.1 33.7 3.0 4.1	0.6 2.0 0.9 1.3	0.0 0.0 0.0 0.0	62.1 3.1 60.1 58.0	11.0 0.0 10.9 9.0	0.0 0.0 0.0 0.2	0.0 0.0 0.0 0.3	Molybdenum & Tungsten 5-6% by weight as sulfides
XXXI-98 0.0240 1340°K 770°K	FROZEN EQUILIBRIUM NON-EQUILIBRIUM EXPERIMENTAL	26.2 62.6 28.4 29.2	5.5 1.4 6.5 11.1	2.9 33.1 6.9 8.7	0.8 1.0 1.5 3.6	0.0 0.0 0.0 0.0	52.7 1.9 45.2 38.0	11.9 0.0 11.4 8.8	0.0 0.0 0.0 0.3	0.0 0.0 0.2 0.3	as above
XXXII-99 0.0245 1280°K 730°K	FROZEN EQUILIBRIUM NON-EQUILIBRIUM EXPERIMENTAL	25.4 62.6 26.3 27.6	5.4 1.4 6.3 7.2	2.8 33.1 5.0 6.6	0.8 1.0 1.4 2.6	0.0 0.0 0.0 0.0	53.9 1.9 49.6 45.2	11.7 0.0 11.5 10.2	0.0 0.0 0.0 0.2	0.0 0.0 0.1 0.4	as above
XXXII-100 0.0490 1330°K 750°K	FROZEN EQUILIBRIUM NON-EQUILIBRIUM EXPERIMENTAL	14.0 62.6 15.2 16.6	2.3 1.4 2.4 3.2	1.5 33.1 2.8 3.7	0.4 1.0 0.6 0.8	0.0 0.0 0.0 0.0	69.4 1.9 66.8 64.0	12.4 0.0 12.2 10.8	0.0 0.0 0.0 0.4	0.0 0.0 0.0 0.5	as above

Table 15. Flow of Pyrolysis Products Through Porous Graphite. Comparison of the Exit Gas Composition for Molybdenum-Tungsten Catalysed and Non-Catalyst Experiments.

RUN NUMBER MASS FLUX FRONT TEMP BACK TEMP	FLOW MODEL	H_2 MOLE %	CH_4 MOLE %	CO MOLE %	CO_2 MOLE %	N_2 MOLE %	H_2O MOLE %	C_6H_6O MOLE %	C_2H_4 MOLE %	C_2H_2 MOLE %	CATALYST
XXVIII-92	FROZEN	27.5	5.3	3.1	1.0	0.0	52.5	10.6	0.0	0.0	
0.0220	EQUILIBRIUM	62.5	1.2	33.9	0.8	0.0	1.6	0.0	0.0	0.0	no
1325°K	NON-EQUILIBRIUM	29.3	7.7	8.0	2.5	0.0	42.2	10.1	0.0	0.2	catalyst
855°K	EXPERIMENTAL	30.0	8.7	8.0	3.4	0.0	37.9	11.6	0.2	0.2	
XXIX-94	FROZEN	25.6	4.1	2.9	0.8	0.0	55.2	11.5	0.0	0.0	
0.0250	EQUILIBRIUM	61.8	1.1	34.9	0.7	0.0	1.5	0.0	0.0	0.0	no
1325°K	NON-EQUILIBRIUM	28.1	5.8	7.8	2.1	0.0	45.1	10.9	0.0	0.3	catalyst
760°K	EXPERIMENTAL	25.5	5.8	10.5	2.7	0.0	42.7	12.2	0.2	0.2	
XXXI-98	FROZEN	26.2	5.5	2.9	0.8	0.0	52.7	11.9	0.0	0.0	Molybdenum
0.0240	EQUILIBRIUM	62.6	1.4	33.1	1.0	0.0	1.9	0.0	0.0	0.0	Tungsten
1340°K	NON-EQUILIBRIUM	28.4	6.5	6.9	1.5	0.0	45.2	11.4	0.0	0.2	5-6% (wt)
770°K	EXPERIMENTAL	29.2	11.1	8.7	3.6	0.0	38.0	8.8	0.3	0.3	as sulfide
XXXII-99	FROZEN	25.5	5.3	2.8	0.8	0.0	53.9	11.7	0.0	0.0	Molybdenum
0.0245	EQUILIBRIUM	62.6	1.4	33.1	1.0	0.0	1.9	0.0	0.0	0.0	Tungsten
1290°K	NON-EQUILIBRIUM	26.3	6.3	5.0	1.4	0.0	49.6	11.5	0.0	0.1	5-6% (wt)
720°K	EXPERIMENTAL	27.6	7.2	6.6	2.6	0.0	45.2	10.2	0.2	0.4	as sulfide

The use of bromine (or HBr) as a representative homogeneous catalyst made a detailed investigation unnecessary because of the relative activity of various halides to hydrogen bromine in Table 11. By comparison, iodine and organic iodide should have a greater influence on the pyrolysis product reactions, while chlorine or the organic chlorides should have a less influence.

No detectable change in the exit product composition, and, therefore, in the rates of chemical reaction of the pyrolysis products, were observed for tungsten and molybdenum co-catalysts and platinum over a temperature range of 1845° to 2300°F (1280°K to 1535°K).

SECTION V

CONCLUSIONS

Based on the experimental and theoretical results of this research the following conclusions are drawn:

The reacting flow of pyrolysis products from nylon-phenolic resin composites in the char zone was accurately described by a finite-rate, reacting flow model. This was confirmed for the simulated pyrolysis product compositions in Table 6, mass flux values between 0.00003 - 0.10 lb/ft^2-sec (0.0015 - 0.5 Kg/m^2-sec), front surface temperatures in the range of 1350 - 2300°F (1000°K - 1535°K), and the reactions and associated kinetic data in Table 5. Results are presented up to a front surface temperature of 3000°F (1925°K). Above this temperature, additional reactions must be considered to accurately describe the chemically reacting flow.

Under conditions of high mass fluxes ($>$0.05 Kg/m^2-sec) and/or low temperatures ($<$1365°K), the flow of pyrolysis products is essentially frozen. These conditions define the upper limit of frozen flow.

The equilibrium flow model erroneously predicts the behavior in the char for all conditions except those in which the mass flux rate is smaller than 0.0001 lb/ft^2-sec (0.0005 Kg/m^2-sec). Mass flux rates greater than this value require the use of a non-equilibrium flow analysis to accurately describe the changes in the chemical composition of the pyrolysis gases as they flow through the char.

The same results were obtained for the reacting flow of pyrolysis products in porous graphite. The same important reactions and kinetic data that applied to the low density nylon-phenolic resin chars likewise apply to the graphite between 1350 - 2300°F (1000°K - 1535°K) and 0.00003 - 0.10 lb/ft^2-sec (0.00015 - 0.5 Kg/m^2-sec). This permits the substitution of graphite for the brittle chars in studies requiring post-experimental analyses of the porous media; i.e., carbon deposition

studies.

Carbon is deposited as a result of the thermal degradation of methane and phenol. Deposition starts near the middle of the char (z/L = 0.5) where the temperature is 1400°F (1035°K) and increases uniformly to a maximum value near the front surface at a temperature of 1900°F (1310°K).

The products of methane degradation were determined by comparing radioactive tracer concentration profiles with the gas chromatograms of the exit gases leaving the Char Zone Thermal Environment Simulator. The species identified were carbon monoxide, carbon dioxide, ethylene, acetylene and unreacted methane. Similarly, the products of phenol degradation were determined. The species were identified as methane, carbon monoxide, carbon dioxide and unreacted phenol. The above methods provided excellent supporting evidence that the reactions considered important in the mathematical model were correct.

The effect of adding homogeneous catalysts (such as bromine) to the pyrolysis product stream to accelerate chemical reactions, and therefore, the heat absorption in the system was determined. Bromine produced a catalytic effect which reduced the temperature at which carbon deposition starts from 1400°F (1035°K) to 1200°F (911°K). The temperature of maximum deposition was likewise reduced to 300° F (150°K). A sharp decline in the carbon deposition probably indicated depletion of carbon by reactions with water and/or carbon dioxide.

Molybdenum and tungsten heterogeneous catalysts did not cause a measureable change in the behavior of the system. A slight shift in the carbon deposition profiles was observed, but this change was of the same order as the accuracy of the analytical equipment. Platinum catalyst likewise failed to produce a change from uncatalysed case.

REFERENCES

1. Wakefield, R. M., Landell, J. H. and Dickey, R. R., "Effects of Pyrolysis-Gas Chemical Reactions on Surface Recession of Charring Ablators," AIAA Journal, Vol. 6, No. 2, February 1969, pp. 122-128.

2. Kendall, R. M., Bartlett, E. P. and Rindal, R. A., "A Multi-component Boundary Layer Chemically Coupled to an Ablative Surface," AIAA Journal, Vol. 5, No. 6, June 1967, pp. 1063-1075.

3. Clark, R. K., Flow of Hydrocarbon Gases in Porous Media at Elevated Temperatures, M. S. Thesis, University of Virginia, Charlottesville, Virginia, August 1968, 108 page.

4. April, G. C., Energy Transfer in the Char Zone of an Charring Ablator, Ph. D. Dissertation, Louisiana State University, Baton Rouge, Louisiana, May 1969, 595 pages.

5. del Valle, E. G., Pike, R. W. and April, G. C., "Modeling for a Set of Complex Chemical Reactions at High Temperatures," Sixty-First Annual Meeting of the AIChE, Paper No. 8f, Los Angeles, California, December 1968.

6. April, G. C., Pike, R. W. and del Valle, E. G., "Nonequilibrium Flow and the Kinetics of Chemical Reactions in the Char Zone," J. Macromol. Sci. - Chem., Vol. A3, No. 4, July 1969, pp. 685-704.

7. Sykes, G. F., Jr., "Decomposition Characteristics of a Char-forming Phenolic Polymer Used for Ablative Composites," NASA TN D-3810, February 1967.

8. Sykes, G. F., Jr., Entry Structures Branch, Langley Research Center, Hampton, Virginia. Private Communication to R. W. Pike and G. C. April, March 14, 1968.

9. Beekman, op. cit., 166.

10. Laidler, K. J., Chemical Kinetics, 2nd Ed., McGraw Hill Book Co., New York, 484 (1965).

11. Kondrat'ev, V. N., Chemical Kinetics of Gas Reactions, Pergamon Press, New York, 36 (1964).

12. Laidler, op.cit., 444.

13. Emmett, P. E., Catalysis, Reinhold Publishing Corp., Baltimore, Maryland, 5, 388 (1957).

14. Minkoff, G. J. and C. F. H. Tipper, Chemistry of Combustion Reactions, Butterworths Publishing Co., Ltd., London, 249 (1962).

15. Emmett, op.cit., 5, 184.

16. Emmett, op.cit., 6, 427.

17. Emmett, op.cit., 6, 407.

18. Harrison, D. P. and H. F. Rase, "Nylon-Platinum Catalysts with Unusual Geometric and Selective Characteristics," Industrial and Engineering Chemistry - Fundamentals, 6 (2), 161 (May 1967).

19. Emmett, op.cit., 5, 217.

20. Emmett, op.cit., 6, 486.

21. Emmett, op.cit., 5, 98.

22. Schwab, Georg-Maria, H. S. Taylor and R. Spence, Catlaysis, D. Van Nostrand Co., New York 26-27 (1937).

23. Simons, J. H., Fluorine Chemistry, Volume V, Academic Press, New York, 2, 87 (1964).

24. Laidler, op.cit., 8.

25. Jolles, Z. E., ed., Bromine and Its Compounds, Academic Press, New York 74, 102-3 (1966).

26. Schwab, op.cit., 58.

NASA-Langley, 1971 —— 33 CR-1903